Dicer Loss in Müller Glia Leads to a Defined Sequence of Pathological Events Beginning With Cone Dysfunction

Daniel Larbi,[1] Alexander M. Rief,[1] Seoyoung Kang,[1] Shaoheng Chen,[1] Khulan Batsuuri,[1] Sabine Fuhrmann,[2] Suresh Viswanathan,[3] and Stefanie G. Wohl[1]

[1]Department of Biological and Vision Sciences, The State University of New York College of Optometry, New York, New York, United States
[2]Ophthalmology and Visual Sciences Department, Vanderbilt Eye Institute, Vanderbilt University Medical Center, Nashville, Tennessee, United States
[3]Indiana University School of Optometry, Bloomington, Indiana, United States

Correspondence: Stefanie G. Wohl, Department of Biological and Vision Sciences, The State University of New York College of Optometry, 33 West 42nd Street, New York, NY 10036, USA; swohl@sunyopt.edu.

Received: December 20, 2024
Accepted: February 7, 2025
Published: March 4, 2025

Citation: Larbi D, Rief AM, Kang S, et al. Dicer loss in Müller glia leads to a defined sequence of pathological events beginning with cone dysfunction. *Invest Ophthalmol Vis Sci*. 2025;66(3):7. https://doi.org/10.1167/iovs.66.3.7

Purpose. The loss of Dicer in Müller glia (MG) results in severe photoreceptor degeneration, as it occurs in retinitis pigmentosa or age-related macular degeneration; however, the sequence of events leading to this severe degenerative state is unknown. The aim of this study was to conduct a chronological functional and structural characterization of the pathological events in MG-specific Dicer-conditional knockout (cKO) mice in vivo and histologically.

Methods. To delete Dicer and mature microRNAs (miRNAs) in MG, two conditional Dicer1 knockout mouse strains (Rlbp-CreER:tdTomato:Dicer-cKO$_{MG}$ and Glast-CreER:tdTomato:Dicer-cKO$_{MG}$) were created. Optical coherence tomography (OCT), electroretinograms (ERGs), and histological analyses were conducted to investigate structural and functional changes up to 6 months after Dicer deletion.

Results. Dicer/miRNA loss in MG leads to (1) impairments of the area spanning from the external limiting membrane (ELM) to the retinal pigment epithelium (RPE), (2) cone photoreceptor dysfunction, and (3) retinal remodeling and functional loss of the inner retina at 1, 3, and 6 months after Dicer loss, respectively, in both of the knockout mouse strains. Furthermore, in the Rlbp-CreER:tdTomato:Dicer-cKO$_{MG}$ strain, rod photoreceptor impairment was found 4 months after Dicer depletion (4) accompanied by alteration of RPE integrity (5).

Conclusions. MG Dicer loss in the adult mouse retina impacts cone function prior to any measurable changes in rod function, suggesting a pivotal role for MG Dicer and miRNAs in supporting cone health. A partially impaired RPE, however, seems to accelerate rod degeneration and overall degenerative events.

Keywords: microRNAs, hyperreflective foci, retinal degeneration, OCT, ERG, RPE, mouse

Retinal degenerative diseases, including age-related macular degeneration (AMD) or retinitis pigmentosa (RP), cause vision impairment and eventually lead to blindness. Although many retinal dystrophies can be linked to mutations in specific genes, non-genetic/epigenetic factors also contribute to disease progression.[1–6] MicroRNAs (miRNAs) belong to non-coding RNAs and act as epigenetic factors by repressing translation. They play a role in retinal disease progression and very likely in disease onset and manifestation, as some of them are cell type–specific (see review Zuzic et al.[2]). miRNAs require processing before they obtain their mature functional form, which occurs via special enzyme complexes, including the Dicer complex. Hence, deleting Dicer1 in retinal cells (photoreceptors or MG) or the RPE is a very efficient way to study the role of cell type–specific mature miRNAs.[7–10]

MG are the primary glia in the retina and fulfill a variety of functions in the healthy retina, including but not limited to (1) feeding neurons with lactate, (2) neurotransmitter recycling (via glutamine synthetase), (3) water ion homeostasis (via water pores and ion pumps), (4) structural stability and integrity via their long processes that span the entire tissue and form the internal/inner limiting membrane (ILM) toward the vitreous and external or outer limiting membrane (ELM/OLM) toward the RPE, (5) cone photopigment recycling, and (6) formation of the blood–retinal barrier (BRB) by wrapping blood vessels.[11–18] Because MG have such myriad functions, it is not far fetched to assume that MG impairment would result in devastating outcomes. Indeed, partial elimination of MG via toxins leads to activation of the remaining glia, disruption of the BRB, and photoreceptor loss resembling degenerative diseases such as AMD, diabetic retinopathy, or macular telangiectasia 2 (MacTel2).[19,20] This suggests that MG are not only responders to damage but also potential initiators of retinal degeneration/retinal dystrophies.

We previously established an MG-specific Dicer knockout mouse and showed that the loss of mature miRNAs in the glia leads to a slow-progressing phenotype that resem-

bles retinitis pigmentosa several months after the manipulation.[9] Intriguingly, MG miRNAs were reduced by about 80% as early as 1 month after Dicer deletion.[9,21] The overall retinal histology, however, appeared unaltered at the time. Only occasionally, the tissue seemed to have some enlarged areas (bulgy appearance), but whether a postmortem event caused this outcome was unclear. Furthermore, even 3 months after Dicer loss, the overall retina was histologically intact, with only occasional alterations at the cellular level (MG displacement). Later, though, several substantial alterations were found, including a thin outer nuclear layer (ONL). How this pathophysiological phenotype developed, when it manifested, and whether the RPE contributed to the outcome were, however, not investigated and are not known. Therefore, the aims of this study were (1) to investigate the impact of the loss of Dicer in adult MG with regard to onset, manifestation, and progression of pathophysiological events in the retina; and to (2) elaborate the contribution of the RPE to the pathophysiological phenotype.

We used two MG-specific Dicer knockout strains—the aforementioned Rlbp-CreER:tdTomato:Dicer-cKO$_{MG}$ mouse[9] and a newly generated Glast-CreER:tdTomato:Dicer-cKO$_{MG}$—and conducted spectral-domain optical coherence tomography (SD-OCT) and electroretinography (ERG) coupled with histological analysis. We analyzed the mice at early (1 month after Dicer deletion), intermediate (3–4 months after Dicer deletion), and late stages (6 months after Dicer deletion). We found that the first dysfunction concerned cone photoreceptors, followed by rod loss and functional loss of inner retinal neurons at a late stage. The degenerative events were more accelerated in the Rlbp-CreER:tdTomato:Dicer-cKO$_{MG}$ mouse that also showed partial RPE impairments.

Methods

Animals and Cre Induction

All mice used in this study were housed at the State University of New York, College of Optometry, in accordance with the Institutional Animal Care and Use Committee–approved protocols and ARVO Statement for the Use of Animals in Ophthalmic and Vision Research. The *Rlbp1-CreERT2* strain was obtained from Edward Levine, PhD, Vanderbilt University.[22] The Glast-CreER strain (Tg[Slc1a3-cre/ERT]1Nat, ID 012586, generated by Jeremy Nathans, MD, PhD, Johns Hopkins University), the *R26-stop-flox-CAG-tdTomato* strain (Ai14, #007908), and the Dicer conditional knockout strain (*Dicer$^{f/f}$*, #006001, generated by Brian Harfe, PhD,[23]) were obtained from The Jackson Laboratories (Bar Harbor, ME, USA) to create the following wildtype and Dicer-conditional knockout (cKO) strains: (1) *Rlbp1-CreERT2: stop$^{f/f}$-tdTomato* (referred to as Rlbp-Cre:tdTomato or wildtype) and corresponding (2) *Rlbp1-CreERT2: stop$^{f/f}$-tdTomato*: *Dicer$^{f/f}$* (referred to as Rlbp-Cre:tdTomato:Dicer-cKO$_{MG}$, or abbreviated Rlbp-Cre:Dicer-cKO$_{MG}$), as well as (3) *Glast1-CreER: stop$^{f/f}$-tdTomato* (referred to as Glast-Cre: tdTomato or wildtype) and corresponding (4) *Glast1-CreER: stop$^{f/f}$-tdTomato: Dicer$^{f/f}$* (referred to as Glast-Cre:tdTomato:Dicer-cKO$_{MG}$, or abbreviated Glast-Cre:Dicer-cKO$_{MG}$). Males and females were used. Genotyping was done using the primers listed in Supplementary Table S1. Tamoxifen (Sigma-Aldrich, St. Louis, MO, USA) was administered intraperitoneally at 75 mg/kg in corn oil for 4 consecutive days, for Dicer deletion at P11–14, to initiate the recombination of the floxed alleles. Furthermore, S129 mice (Rlbp1-CreER background strain), tdTomato mice (C57Bl6 background strain), and Cre-negative mice were used as controls and were compared to tamoxifen-treated wildtype mice to exclude the possibility of a treatment effect or any abnormality of the wildtype controls used.

Retinal SD-OCT Imaging

In vivo retinal structure was assessed using the Envisu R2200 SD-OCT device (Bioptigen, Durham, NC, USA). Animals were anesthetized via intraperitoneal injection of 75 to 100 mg/kg ketamine and 5 to 10 mg/kg xylazine dissolved in sterile saline. Pupils were dilated with phenylephrine hydrochloride (2.5%) and tropicamide (0.5%). Corneas were kept lubricated during scans using methylcellulose. Rectangular and radial volume scans (1.4 × 1.4 mm, 1000 A-scans/B-scans × 15 frames/B-scan) were obtained while centered on the optic nerve head. For image analysis, retinal layers were manually segmented in a 9 × 9 plot in four regional quadrants (superior–inferior, nasal–temporal), and thicknesses were measured using the Diver 2.4 software. Total retinal thickness was defined as the distance from the inner border of the retinal nerve fiber layer (NFL) and the outer border of the retinal pigment epithelium (RPE). All nuclear and plexiform layers were analyzed including the NFL/ganglion cell layer (GCL), inner plexiform layer (IPL), inner nuclear layer (INL), outer plexiform layer, and ONL. The region containing the inner and outer segments of photoreceptors and the RPE could not be distinguished with high resolution. Therefore, the distance between the outer border of the ELM (also known as the outer limiting membrane [OLM]) to the outer border of the RPE was consolidated as ELM–RPE area as described previously.[24,25] Thickness measurements were conducted in the central areas, ~650-µm radius from the optic nerve (ON). To create a timeline of thickness changes in different retinal layers, we averaged the thicknesses measured at various retinal eccentricities in both the superior–interior and nasal–temporal directions for each time point of analysis.

Electroretinogram Recordings

Mice were dark adapted overnight and anesthetized via an intraperitoneal injection of 75 to 100 mg/kg ketamine and 5 to 10 mg/kg xylazine dissolved in sterile saline. Recordings were performed in the dark room using the Espion Electrophysiology System (Diagnosys LLC, Lowell, MA, USA). Pupils were dilated with 1% tropicamide ophthalmic solution, and the eyes were lubricated using 1% methylcellulose. Animals were kept on a heat pad during the recording to maintain constant body temperature. The Espion Electrophysiology System uses a gold wire electrode as a recording electrode, with needles inserted into the cheek and back as reference and ground electrodes, respectively; a hand-held portable stimulator is the light source. Fullfield 5-ms flashes were used to elicit responses. ERGs were obtained with light intensities ranging from 0.001 to 64 cd·s/m^2 (scotopic) and 0.06 to 17.5 cd·s/m^2 (photopic). Scotopic and photopic ERG a-wave amplitudes were measured from the baseline of the waveform to the trough of the initial negative deflection, and the b-wave amplitudes were measured from the trough of the initial negative deflection to the peak of the subsequent positive deflection. For an in-depth analysis of the scotopic b-wave, the Naka–Rushton equation was used to fit the intensity–response amplitudes:

$$V(I) = V_{max}\left(I^n\right) / \left(I^n + K^n\right) \quad (1)$$

where I is the stimulus intensity; V is the amplitude at stimulus intensity I; V_{max} is the maximum/saturated amplitude and an indirect measurement for responsiveness; K is the semi-saturation constant and represents the stimulus intensity I at which half of the saturated amplitude V_{max} is reached and hence is an indirect measurement for sensitivity; and n is the slope of the fit curve and an indirect measurement of gain/heterogeneity.[26,27]

Tissue Preparation

Mice were euthanized and eyes were marked at the nasal side, enucleated, and transferred to prechilled phosphate-buffered saline (PBS) for eye cup preparation or Hank's Balanced Salt Solution (HBSS) for RPE preparation.

Retinal Cross-Sections. The eyeball was prefixed in 4% paraformaldehyde (PFA) at 4°C for 20 minutes. After removal of the cornea, lens, iris, and vitreous body in PBS, the eyecups were fixed in cold 4% PFA for an additional 20 minutes, washed for 10 minutes in prechilled PBS, and incubated with 30% sucrose in PBS overnight at 4°C. The tissue was embedded with a nasal–temporal orientation in optimum cutting temperature (OCT) embedding medium and frozen at –80°C. The frozen tissue was cross-sectioned in 12 µm thick sections for subsequent immunofluorescent labeling.

Retinal Flatmounts. The unfixed eyeball was carefully dissected in cold PBS to remove the cornea, lens, iris, ciliary body, and vitreous body. The retina was carefully lifted from the RPE and transferred to a slide. To flatten the retina, four symmetric radial cuts were made. The tissue was subsequently fixed with cold 4% PFA for 20 minutes at room temperature (RT), washed three times for 10 minutes in PBS, and stained.

RPE Flatmounts. RPE preparation was conducted as described before.[28] In brief, muscles and connective tissue on the sclera were removed to facilitate the tissue flattening. Cornea, iris, lens, and vitreous body were removed, and the RPE (with attached retina) was carefully transferred on filter paper. Tissue was cut radially, and the retina was gently separated. The RPE (with sclera) was fixed with cold 4% PFA for up to 2 hours at RT, washed three times in PBS at RT for 10 minutes, and stained.

Immunofluorescent Labeling

For immunofluorescent staining, frozen sections were dried at 37°C for 20 minutes, fixed for 20 minutes with 4% PFA, and washed in PBS. Sections or flatmounts were incubated in blocking solution (5% milk block comprised of 2.5 g nonfat milk powder in 50 mL PBS, with 0.5% Triton X-100 or 5% horse serum with 0.5% Triton X-100) for at least 1 hour at RT. After blocking, the tissue was incubated with primary antibodies (Supplementary Table S2) in 5% milk block or horse serum overnight, and retinal flatmounts were incubated for 2 to 3 days. After three thorough washes in PBS, the tissue was incubated with secondary antibodies (1:500–1000; Supplementary Table S2) for 1 hour (slides) or 1 day (flatmounts) at RT and then counterstained with 4′,6-diamidino-2-phenylindole (DAPI, 1:1,000; Sigma-Aldrich). After incubation, the tissue was washed three times in PBS and mounted with cover glasses and mounting medium (Invitrogen).

Fluorescence Microscopy, Confocal Laser Scanning Microscopy, and Image Processing

For whole tissue imaging, retinal eye cups were imaged using a fluorescent microscope (Keyence, Indianapolis, IN, USA) equipped with a 4× objective. Immunofluorescent-labeled retinal cross-sections, RPE flatmounts, and retinal flatmounts were imaged using a confocal laser scanning microscope (Fluoview FV1200; Olympus, Tokyo, Japan) equipped with 4×, 10×, 20×, or 40× objectives and Fluoview FV31S software. Images were processed and analyzed using Adobe Bridge and Photoshop (Adobe, San Jose, CA, USA) and Affinity software (West Bridgford, UK).

Statistical Analysis

Statistical analyses were performed using the Mann–Whitney U test. The Holm–Bonferroni method was used to correct for multiple comparisons. $P < 0.05$ was considered significant.

Results

The MG-Specific Rlbp-Cre:Dicer-cKO$_{MG}$ Mouse Is a Reliable Mouse Model Resulting in a Robust Phenotype Resembling Retinal Degenerative Diseases

In order to perform an in vivo in-depth analysis of retinal health and function in the MG-specific Dicer-cKO mouse model (referred to as Rlbp-Cre:Dicer-cKO$_{MG}$),[9] we first validated the establishment of the reported phenotype. Tamoxifen was injected on postnatal days 11 to 14 (P11–P14)[9] to activate the Cre recombinase, and the tissue was evaluated histologically 1 and 6 months after Dicer deletion (Fig. 1A). The wildtype showed sufficient reporter induction (~98%) in glutamine synthetase (GS) and Sox9 expressing MG (Figs. 1B–1G), consistent with previous reports.[9,29] The retinas of the 1-month-old Rlbp-Cre:Dicer-cKO$_{MG}$ showed complete reporter induction throughout the retina, as well as the previously reported random areas with somewhat dislocated MG (Figs. 1H–1J). In the retinas of the 6-month-old Dicer-cKO$_{MG}$ mice, severe disruptions and thinning of the central areas were found, predominantly in the ONL, confirming the reported phenotype.[9] The MG appeared to form a large glial seal (Figs. 1K, 1L, arrowheads) resembling the events reported in late-stage retinal remodeling[30] and had reduced glutamine synthase labeling (Fig. 1M, arrows), a hallmark of specific gliosis.[30] Furthermore, the RPE seemed to interact with the ELM/retina (Fig. 1K, arrows), a process that appears to occur in a variety of retinal diseases with photoreceptor loss.[31,32] Hence, all previously reported features of this mouse model were present, confirming the robust and reliable phenotype and allowing an in-depth in vivo structural and functional analysis to elaborate the sequence of events leading to this severe degenerative state.

miRNA Loss in Müller Glia Does Not Result in Substantial Structural or Functional Retinal Impairment in the Early Phase But Leads to Some Alterations in the ELM–RPE and INL

To investigate structural abnormalities in vivo, we conducted SD-OCT 1 month after Dicer deletion, the time point by

Investigative Ophthalmology & Visual Science

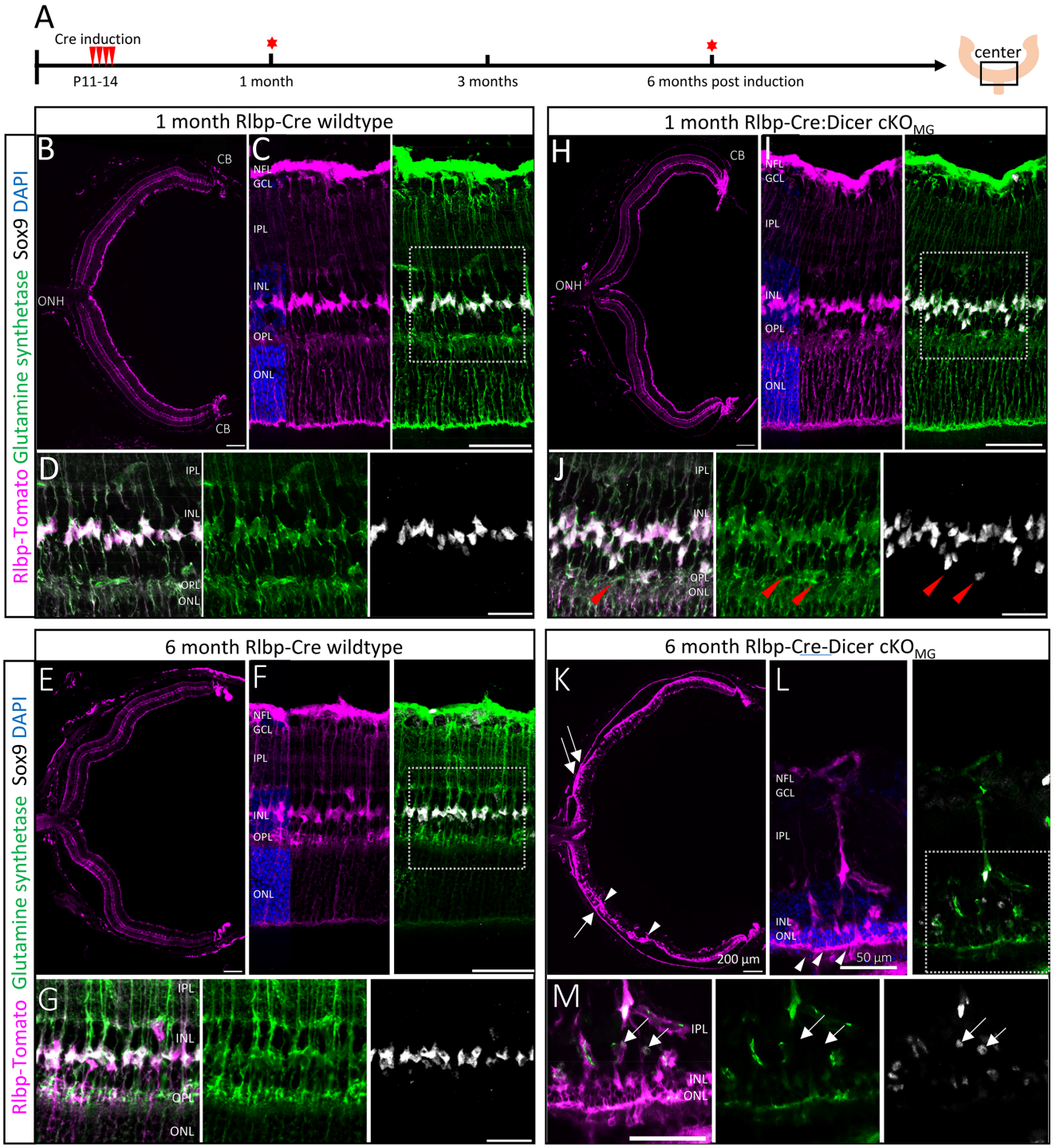

Figure 1. miRNA loss in MG results in retinal degeneration at late stage. (**A**) Experimental design showing Cre activation at P11 to P14 and time points of analysis 1 and 6 months after Cre induction (*red stars*). (**B–M**) Immunofluorescent labeling with antibodies against RFP (Rlbp1:Tomato), glutamine synthetase (GS), and SOX9, as well as DAPI nuclear staining of center areas of Rlbp-Cre wildtype (WT) mice (**B–G**) or Rlbp-Cre:Dicer-cKO$_{MG}$ mice (**H–M**), 1 or 6 months after Cre induction. The insets in **C**, **F**, **I**, and **L** are shown in **D**, **G**, **J**, and **M**, respectively. *Red arrowheads* in **J** indicate displaced MG. *Arrows* in **K** show RPE–ELM interactions. *Arrowheads* in **K** and **L** show MG seal formation. *Arrows* in **M** show GS-negative cells. *Scale bars*: 200 µm (**B**, **E**, **H**, **K**), 50 µm (**C**, **F**, **I**, **L**), 25 µm (**D**, **G**, **J**, **M**).

which ~70% to 80% of all miRNAs are reduced[9,21] (Fig. 2A). Thickness measurements for whole retinal thickness and the individual layers were conducted in the central areas (~650-µm radius from the ON, across the nasal–temporal and superior–inferior axes) (Fig. 2D; Supplementary Figs. S1A, S2A).

OCT scans of wildtype and Rlbp-Cre:Dicer-cKO$_{MG}$ 1 month after Cre induction did not show any substan-

Investigative Ophthalmology & Visual Science

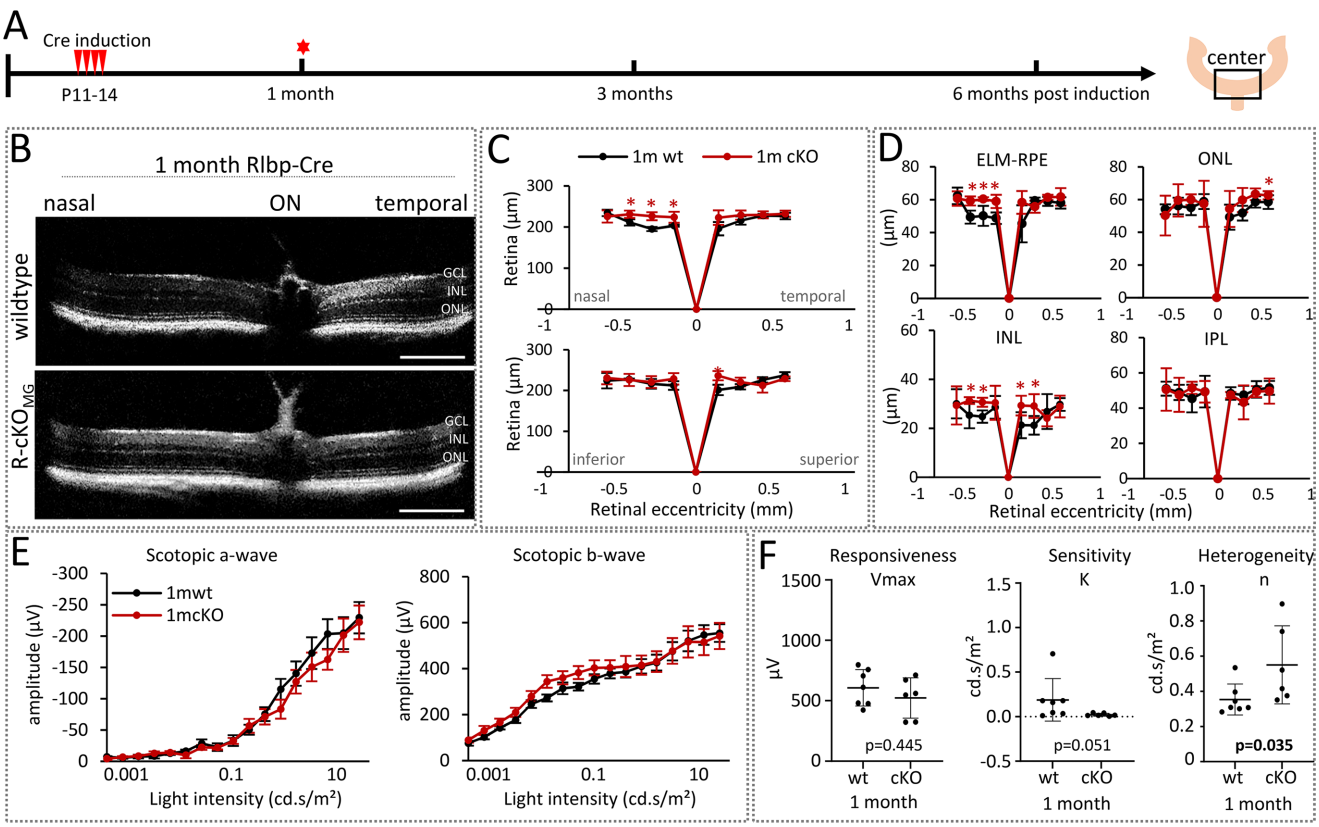

Figure 2. Early-stage MG alterations have no impact on retinal structure and function. (**A**) Experimental design. (**B**) OCT images of WT and Rlbp-Cre:Dicer-cKO$_{MG}$ (R-cKO$_{MG}$, cKO) center retinas (1300-µm diameter) at the nasal–temporal axis 1 month after Cre induction. (**C**) Spider plots of the overall retinal thickness (diameter, µm) measured at the nasal–temporal and superior–inferior axes of WT mice ($n = 4$) and Rlbp-Cre:Dicer-cKO$_{MG}$ mice ($n = 6$). (**D**) Spider plots of the thickness (µm) of the ELM–RPE, ONL, INL, and IPL. (**E**) Fullfield scotopic ERG recordings showing a-wave and b-wave amplitudes of WT mice ($n = 7$) and Rlbp-Cre:Dicer-cKO$_{MG}$ mice ($n = 6$) 1 month after Cre induction. (**F**) Estimated saturated amplitudes (V_{max}, responsiveness), semi-saturation (K, sensitivity), and slope (n, heterogeneity) using the Naka–Rushton equation. OCT shown as mean ± SD; ERG shown as mean ± SEM. Significant differences are indicated. *$P \leq 0.05$, Mann–Whitney U test. *Scale bars*: 200 µm (**B**). Layer explanation is given in Figure 1.

tial abnormalities. The overall retinal thickness was about 215 µm for both conditions, which equals the thickness of a normal mouse retina.[33–35] Some nasal areas in the Rlbp-Cre:Dicer-cKO$_{MG}$ retinas were, however, ~10% thicker than the wildtype, caused by an enlarged nasal ELM–RPE area (Figs. 2C, 2D; Supplementary Fig. S1A). This suggests a possible dilatation due to a swelling of MG endfeet (ELM enlargement), fluid build-up (or both), or a possible RPE enlargement. Furthermore, the INL was increased (~10 µm) (Fig. 2D, Supplementary Fig. S1A), an event known to occur in human RP.[36–38]

Next, we conducted scotopic ERGs but no rod photoreceptor (a-wave amplitudes) or rod bipolar cell (b-wave amplitudes) impairments were present 1 month after Dicer deletion, (Fig. 2E). We then performed an in-depth analysis using the Naka–Rushton equation.[39] This equation allows the evaluation of responsiveness of the tissue via the saturated amplitude (V_{max}), sensitivity via the semi-saturation constant (K), and heterogeneity via slope (n) (Fig. 2F). Although there was no difference in the responsiveness and sensitivity in the b-wave response of Rlbp-Cre:Dicer-cKO$_{MG}$ mice, the slope was different. This indicates patchy functional impairments, which are known features in early stages of retinal dystrophies with drastic photoreceptor loss such as RP.[40,41]

Initial Structural Abnormalities, Indicated by Hyperreflective Foci and Photoreceptor Layer Thinning, Do Not Result in Functional Impairment 3 Months After Dicer Deletion

We next analyzed the retinas of Rlbp-Cre:Dicer-cKO$_{MG}$ mice 3 months after Dicer deletion and compared it to age-matched wildtypes (Fig. 3A). No differences in the overall retinal thickness or the particular layer thicknesses were found (Figs. 3B–3D; Supplementary Figs. S1B, S2B). However, about 40% of all mice analyzed displayed hyperreflective foci in the ELM–RPE or outer plexiform layer (OPL) (Fig. 3B, arrowheads). These foci are often cell accumulations (microglia)[19] or small detachments caused by fluid build-up.[42–45] Because we could not confirm microglia or macrophage accumulation in retinal cross-sections, the foci could be a consequence of the ELM enlargement we found in the 1-month Rlbp-Cre:Dicer-cKO$_{MG}$ mice. Furthermore, despite an overall preserved thickness, there was an initial reduction of the ELM–RPE region in the temporal central cKO retina (Fig. 3D), indicating a possible initial photoceptor impairment. The INL in the 3-month Rlbp-Cre:Dicer-cKO$_{MG}$ mice was back to normal size (Fig. 3D; Supplementary Figs. S1B, S2B).

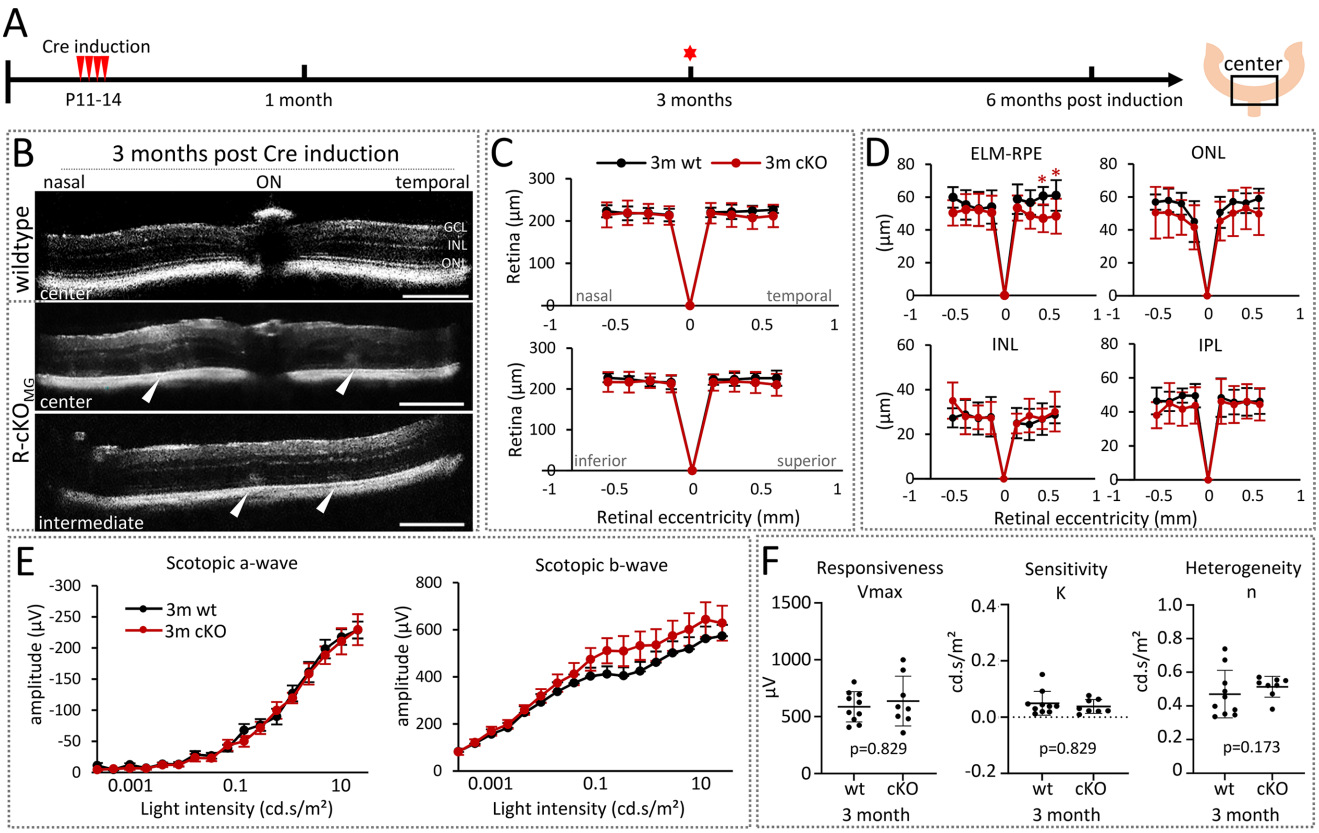

Figure 3. Intermediate-stage retinas display structural abnormalities but no functional impairments. (**A**) Experimental design. (**B**) OCT images of WT or Rlbp-Cre:Dicer-cKO$_{MG}$ mice (R-cKO$_{MG}$, cKO, center retinas, 1300-µm diameter) 3 months after Cre induction at the nasal–temporal axis. *Arrowheads* indicate hyperreflective foci. (**C**) Spider plots of the overall retinal thickness (diameter, µm) measured at the nasal–temporal and superior–inferior axes of WT mice ($n = 7$) and Rlbp-Cre:Dicer-cKO$_{MG}$ mice ($n = 11$). (**D**) Spider plots of the thickness (µm) of the ELM–RPE, ONL, INL, and IPL. (**E**) Fullfield scotopic ERG recordings showing a-wave and b-wave amplitudes of WT mice ($n = 10$) and Rlbp-Cre:Dicer-cKO$_{MG}$ mice ($n = 8$). (**F**) Estimated maximum amplitudes (V_{max}, responsiveness), semi-saturation (K, sensitivity), and slope (n, heterogeneity) using the Naka–Rushton equation. OCT shown as mean ± SD; ERG shown as mean ± SEM. Significant differences are indicated. *$P \leq 0.05$, Mann–Whitney U test. *Scale bars*: 200 µm (**B**). Layer explanation is given in Figure 1.

Despite these initial structural alterations, scotopic ERGs showed no signs of neuronal impairment (Fig. 3E); however, we found a trend toward a slightly higher amplitude of the scotopic b-wave in the Rlbp-Cre:Dicer-cKO$_{MG}$ retinas. V_{max}, semi-saturation K, and slope n did not differ from wildtype retinas. This shows not only no functional impairment at this intermediate stage but also the offset of the differences in heterogeneity found in the early stages, which appear to be transient (Fig. 3F vs. Fig. 2F).

Dicer Loss in Müller Glia Leads to Significant Neuronal Functional Loss in Outer and Inner Retina at Late Stage

Next, we analyzed the late phase and conducted OCT measurements 6 months after Cre induction (Dicer/miRNA loss). We found a significantly progressed phenotype regarding pathophysiological features and functional impairment (Fig. 4; Supplementary Figs. S1C, S2C). The retinas of the Rlbp-Cre:Dicer-cKO$_{MG}$ mice were thinner and displayed more hyperreflective foci. These foci seemed to be more defined (less cloudy), particularly between the ELM and RPE (Fig. 4B, arrows). Compared to age-matched wildtype mice, retinas of the Rlbp-Cre:Dicer-cKO$_{MG}$ mice displayed an approximately 20% reduction of the overall retinal thickness (Figs. 4C, 4D), independent of orientation. The most prominent reduction was seen in the ELM–RPE and the ONL reflecting photoreceptor loss. Interestingly, the inner layers were unchanged or slightly thicker (Fig. 4D; Supplementary Figs. S1C, S2C). This severe pathological phenotype was accompanied by a significantly reduced scotopic a-wave and b-wave (Fig. 4E). The V_{max} (saturated amplitude) was significantly reduced, indicating reduced retinal responsiveness in the 6-month Dicer-cKO$_{MG}$ and potential inner retinal defects (Fig. 4F).

Immunofluorescent labeling using antibodies against calbindin to label horizontal cells (HCs) and amacrine cells (ACs), as well as calretinin (ACs) and choline acetyltransferase (ChAT, ACs), confirmed inner retinal defects (Fig. 5). These markers also label retinal ganglion cells and displaced ACs in the GCL, but no impairments were seen in this layer (Figs. 5B–5G). We found severe disruptions of the neuronal circuitry in 6-month Rlbp-Cre:Dicer-cKO$_{MG}$ retinas, with some neuronal cell bodies being located beneath the glial seal in the outer retina (Fig. 5E, yellow arrow). Similar events occur during late-stage retinal remodeling in AMD or RP.[30,46–48] This indicates that the MG-driven retinal degeneration patterns found in the late-stage Rlbp-Cre:Dicer-cKO$_{MG}$ mouse do indeed resemble those of non–glia-based retinal

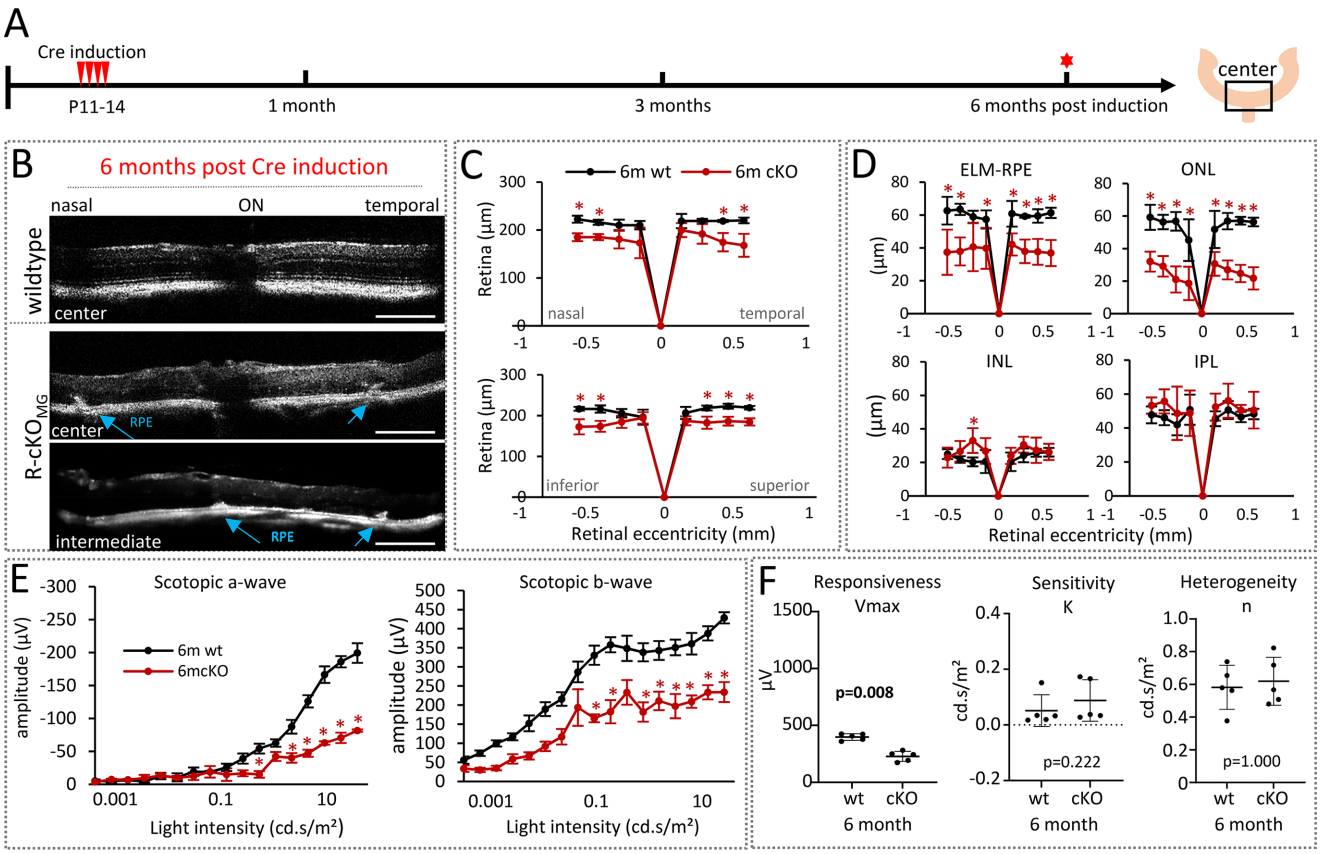

Figure 4. The miRNA-depleted MG cause photoreceptor loss and vision impairment at the late stage. (**A**) Experimental design. (**B**) OCT images of WT or Rlbp-Cre:Dicer-cKO$_{MG}$ mice (R-cKO$_{MG}$, cKO, center retinas; 1300-µm diameter) 6 months after Cre induction at the nasal–temporal axis. *Arrows* indicate hyperreflective foci. (**C**) Spider plots of the overall retinal thickness (diameter, µm) measured at the nasal–temporal and superior–inferior axes of WT mice ($n = 4$) and Rlbp-Cre:Dicer-cKO$_{MG}$ mice ($n = 7$). (**D**) Spider plots of the thickness (µm) of the ELM–RPE, ONL, INL, and IPL. (**E**) Fullfield scotopic ERG recordings showing a-wave and b-wave amplitudes of WT mice ($n = 5$) and Rlbp-Cre:Dicer-cKO$_{MG}$ mice ($n = 5$) 6 months after Cre induction. (**F**) Estimated maximum amplitudes (V_{max}, responsiveness), semi-saturation (K, sensitivity), and slope (n, heterogeneity) using the Naka–Rushton equation. OCT shown as mean ± SD; ERG shown as mean ± SEM. Significant differences are indicated. *$P \leq 0.05$, Mann–Whitney U test. *Scale bars*: 200 µm (**B**). Layer explanation is given in Figure 1.

degenerative models. These patterns also include the glial seal formation and the RPE alterations (Figs. 5E–5G, arrowheads and white arrow, respectively). In particular the RPE appeared to grow inside the retina by forming quite noticeable invaginations. These invaginations resembled the shape of the hyperreflective foci seen in the OCT scans (Fig. 5E, inset, red arrow).

Initial Rod Photoreceptor Degeneration Is Observed at 4 Months After miRNA Loss in Müller Glia

To decipher the events happening between the intermediate stage (3 months) and late stage (6 months) and to determine the time point of neuronal cell and neuronal functional loss, we conducted OCT and ERG at 4 and 5 months after Dicer deletion (Fig. 6A). OCT scans of 4-month Rlbp-Cre:Dicer-cKO$_{MG}$ retinas showed many hyperreflective foci (cloudy appearance), predominantly in the space between the ELM and the RPE, reflecting pathogenesis progression (Fig. 6B, arrowheads). Thickness measurements displayed initial retinal thinning in both orientations (Fig. 6C; Supplementary Figs. S1D, S2D, orange graphs). The most affected layer was the ONL (photoreceptor loss) and to a lesser extent in the ELM–RPE area (unchanged compared to the 3-month time point) (Figs. 6D, 6E).

OCT scans from 5-month Rlbp-Cre:Dicer-cKO$_{MG}$ retinas showed less hyperreflective foci in the area between the ELM and RPE (Fig. 6E, arrowheads), suggesting a possible reduction of fluid build-up in this area. However, the retinal lamination appeared to be altered, and in particular the IPL appeared enlarged, at least in some areas (Fig. 6B, arrows). The measurements of the retinal layers showed significant thinning of the total retina, especially of the ONL and the ELM–RPE area, indicating progressed photoreceptor loss (Figs. 6C, 6D, red graphs). A time course of the overall structural alterations in the Dicer-cKO (averaged measurements across the nasal–temporal and superior–inferior axes) is given in Figure 6F. The ELM–RPE area began to decrease 3 months after Dicer deletion (~35% declined by 6 months compared to the wildtype baseline). This ELM–RPE alteration went hand in hand with the decrease of the ONL thickness, evident 4 months after Dicer deletion (50% reduction by 6 months compared to the wildtype baseline) (Fig. 6F). Conversely, the IPL increased in thickness beginning 4 months after Dicer deletion and maintained this thickness until late stage, despite remodeling or perhaps because of it. The other layers remained unaffected (Supplementary Fig. S3A).

Investigative Ophthalmology & Visual Science

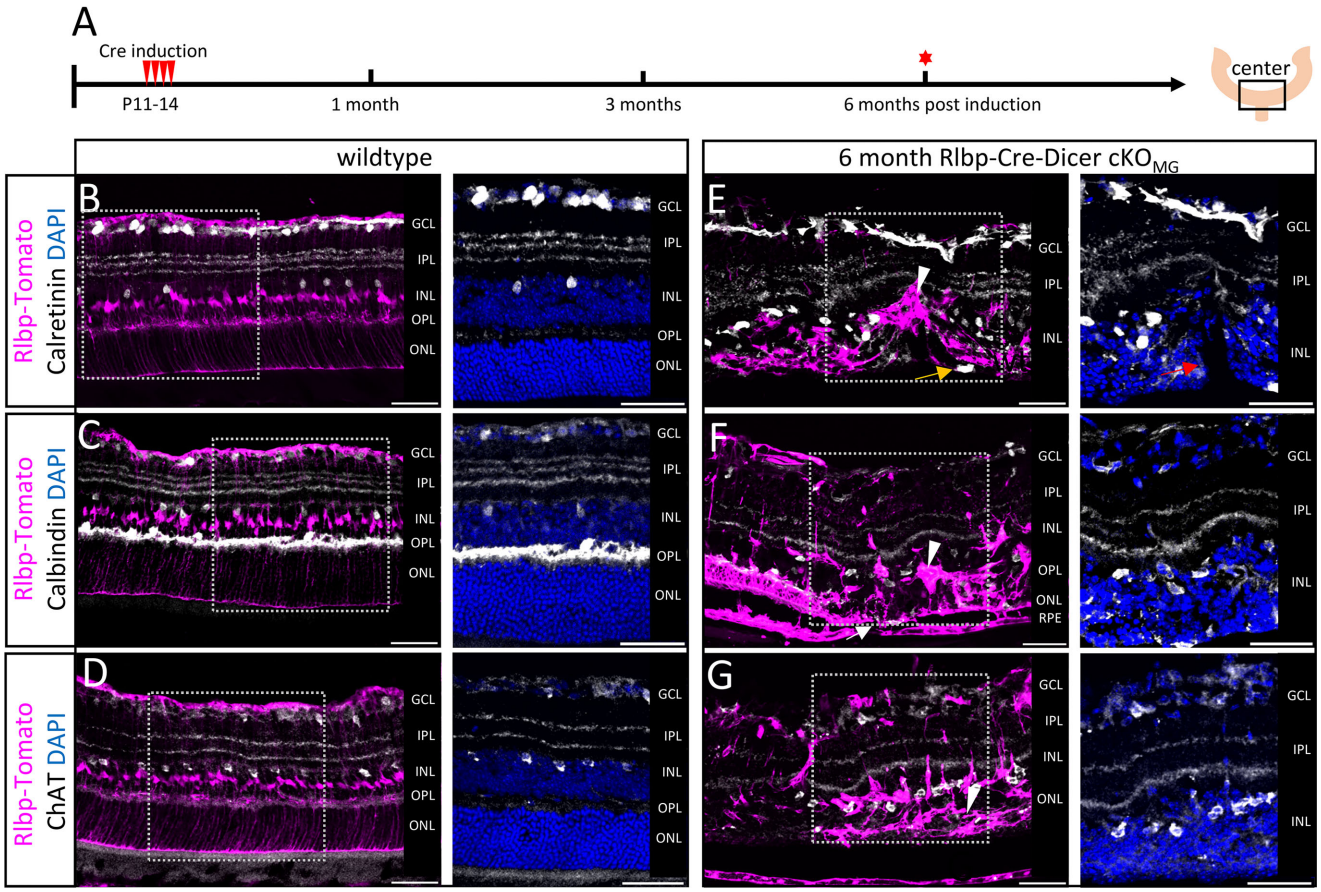

Figure 5. Retinal remodeling in late-stage retinas with miRNA-depleted MG. (**A**) Experimental design. (**B–G**) Immunofluorescent labeling with antibodies against RFP (Rlbp1:Tomato), calretinin (**B**, **E**), calbindin (**C**, **F**), and ChAT (**D**, **G**), as well as DAPI nuclear staining of center areas of WT mice (**B–D**) or Rlbp-Cre:Dicer-cKO$_{MG}$ mice (**E–G**), 6 months after Cre induction. *Arrowheads* in **E**, **F**, and **G** show a glial seal; the *yellow arrow* in **E** indicates a neuronal cell body beneath the glial seal; the *red arrow* in the high-magnification inset in **E** shows invagination; the *white arrow* in **F** indicates RPE–ELM interaction/fusion. *Scale bars*: 50 µm. Layer explanation is given in Figure 1.

ERGs conducted 4 months after Dicer deletion showed a significant reduction in the scotopic a-wave amplitude relative to wildtype, confirming a decline in functional integrity of the retina at this stage (Fig. 6G). This loss of rod function correlates with the thinning in ONL and ELM–RPE observed in OCT; however, the scotopic b-wave, an indicator of rod bipolar cell and MG function was not impaired, although a slight trend toward a reduced b-wave response was found (Fig. 6G). The in-depth analysis of the b-wave response using Naka–Rushton equation showed that responsiveness (V_{max}), sensitivity (K), and heterogeneity (slope n) were not altered at this stage (Fig. 6H). The time course of the scotopic a-wave and b-wave ranging from 1 to 6 months after Dicer deletion and the time course of the Naka–Rushton parameters are given in Supplementary Figs. S3B and S3C, showing the first functional rod deficit 4 months after Dicer deletion.

The Loss of Cone Function Precedes the Loss of Rod Function

Because MG play an essential role in cone pigment recycling, we next measured the photopic b-wave response 3, 4, and 6 months after Dicer deletion to analyze cone health in the cKO mouse (Fig. 7A). A photopic a-wave is not detectable in rodents due to a small cone population.[49,50] We found that cone loss preceded rod loss; 3 months after Dicer deletion, the photopic b-wave amplitude in the cKO was reduced by ~20% compared to age-matched wildtypes and further dropped with age (Figs. 7B–7D). Immunofluorescent labeling with antibodies against M opsin showed less dense cone outer segments in cKO retinas that also appeared scattered or fragmented, validating the functional deficit (Figs. 7E–7H', arrowheads).

The Loss of miRNAs in the RPE Causes Partial RPE Alteration

Because Rlbp1 is expressed not only in MG but also in the RPE, a contribution of a malfunctioning RPE to the observed rod loss in the Dicer-cKO$_{MG}$ mouse cannot be ruled out. We therefore labeled flatmounted RPE with zonula occludens 1 (ZO-1), a marker for tight junctions of the RPE,[51] and orthodenticle homeobox 2 (OTX2), a marker known to be expressed in mature RPE.[52,53] wildtype and cKO RPE displayed a mosaic expression, in agreement with previous reports.[22,54] Some animals had about 70% reporter induction, whereas others had only about 40%. Wildtype RPE cells and reporter negative cells in the cKO were healthy, displaying defined ZO-1–labeled membranes and one or two OTX2^{+} nuclei in the center of the cell (Figs. 8A, 8A').

Investigative Ophthalmology & Visual Science

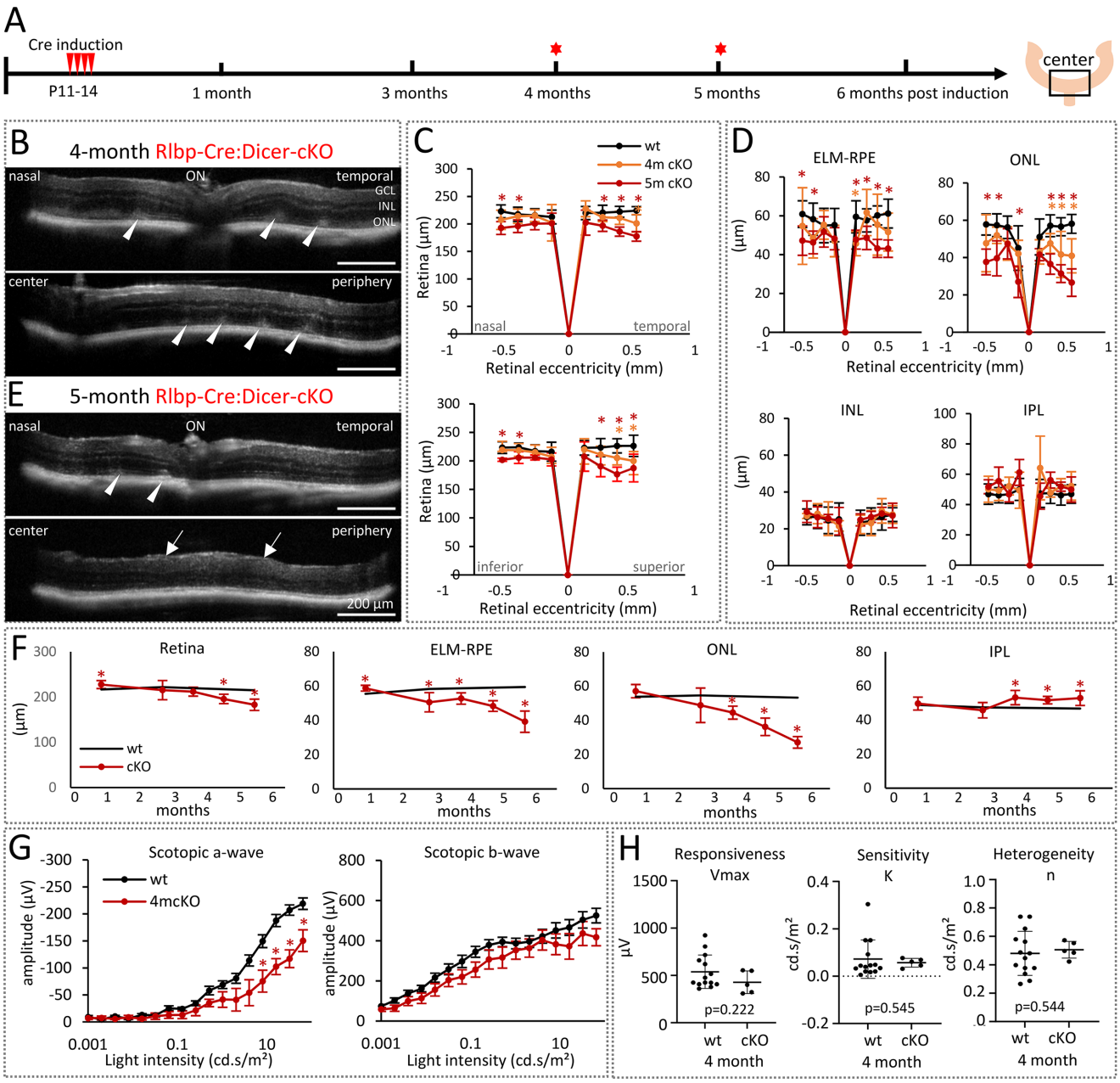

Figure 6. Rod functional impairments are evident 4 months after MG miRNA depletion. (**A**) Experimental design. (**B**, **E**) OCT images of central and peripheral retinal areas of Rlbp-Cre:Dicer-cKO$_{MG}$ mice 4 months (**B**) and 5 months (**E**) after Cre induction. *Arrowheads* indicate structural impairments, and *arrows* indicate enlarged INL. (**C**) Spider plots of the overall retinal thickness at the nasal–temporal and superior–inferior axes of WT mice ($n = 11$), 4-month mice ($n = 5$), and 5-month Rlbp-Cre:Dicer-cKO$_{MG}$ mice ($n = 5$). (**D**) Spider plots of the thickness (µm) of the ELM–RPE, ONL, INL, and IPL. (**F**) Timeline plots showing the averaged thickness of Rlbp-Cre:Dicer-cKO$_{MG}$ mice over time for the total retinal and specific layers. (**G**) Fullfield scotopic electroretinogram recordings showing a-wave and b-wave amplitudes of 4-month Rlbp-Cre:Dicer-cKO$_{MG}$ mice ($n = 5$) in comparison to WT mice ($n = 15$). (**H**) Estimated maximum amplitudes (V_{max}, responsiveness) semi-saturation (K, sensitivity), and slope (n, heterogeneity) using the Naka–Rushton equation. OCT shown as mean ± SD; ERG shown as mean ± SEM. Significant differences are indicated. *$P \leq 0.05$, Mann–Whitney U test. *Scale bars*: 200 µm (**B**, **E**). Layer explanation is given in Figure 1.

Three-month cKO RPE cells, however, had less intense ZO-1 and OTX2 labeling and dislocated nuclei (toward the cell membrane) (Figs. 8B, 8B', arrows). These dislocated nuclei appeared to be smaller and were mostly arranged in pairs. Some cells seemed to have several nuclei, suggesting either cell division or a potential nuclear migration. Six-month cKO RPE cells displayed a more progressed phenotype, as many cells displayed very weak ZO-1 expression in the cell membrane and faint OTX2$^+$ or OTX2$^-$ nuclei (Figs. 8C, 8C', arrowheads), indicating impaired RPE. Interestingly, the RPE of cKO mice had also tdTomato (reporter)-negative "normal" RPE cells (mosaic expression). They displayed mostly wildtype-like ZO-1 and OTX2 expression patterns. However, some of these normal (reporter-negative) RPE cells appeared to be enlarged with partly absent ZO-1$^+$ membranes (Fig. 8C, arrows). This may suggest a possible

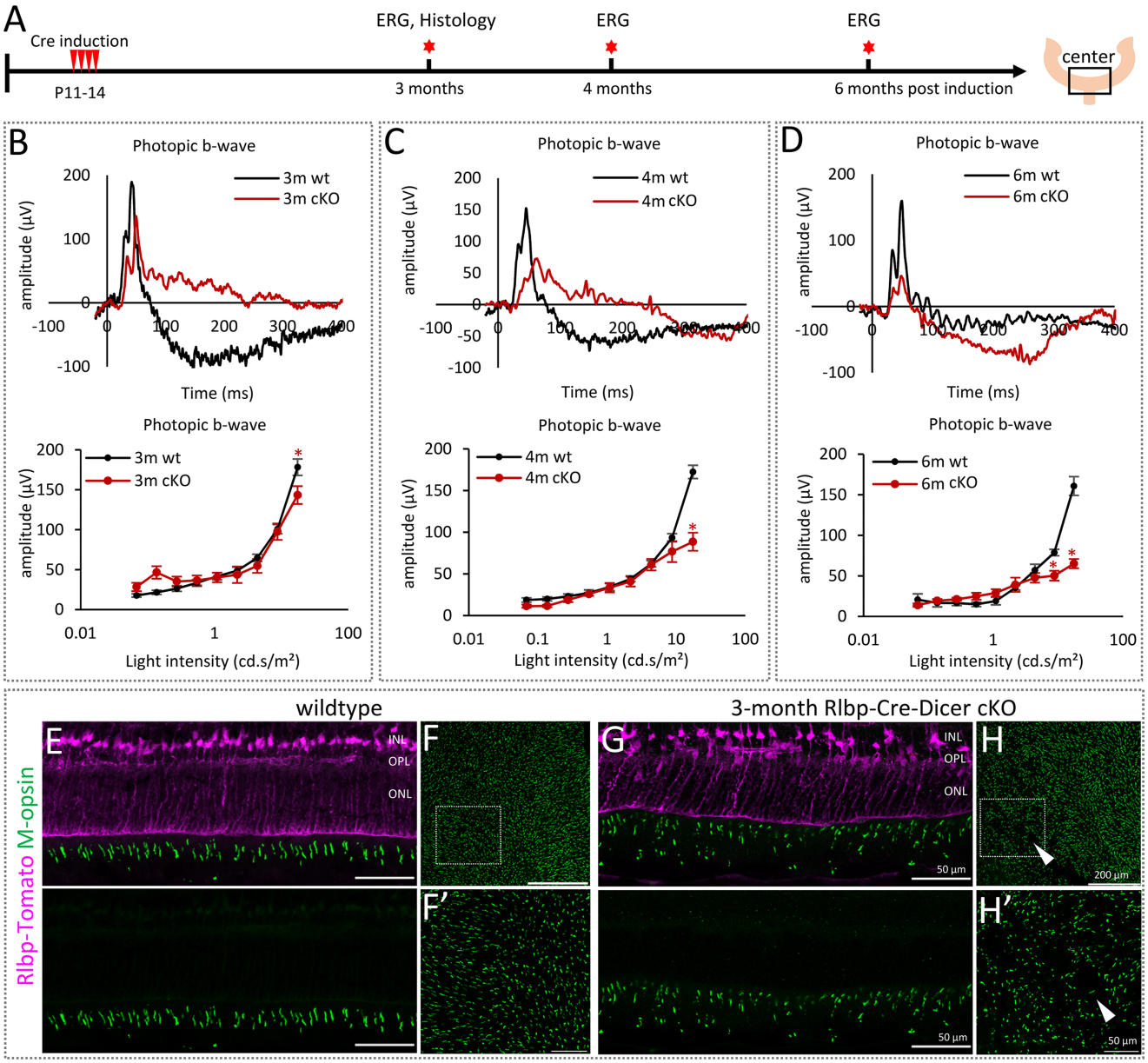

Figure 7. Rlbp-Cre:Dicer-cKO mice display loss of cone function 3 month after Cre induction. (**A**) Experimental design. (**B–D**) Fullfield photopic ERG recordings showing representative ERG waveforms and b-wave intensity–amplitude plots for WT and Rlbp-Cre:Dicer-cKO$_{MG}$ mice at 3 months (WT, $n = 10$; cKO, $n = 8$) (**B**), 4 months (WT, $n = 15$; cKO, $n = 5$) (**C**), and 6 months (WT, $n = 5$; cKO, $n = 5$) (**D**). (**E–H'**) Immunofluorescent labeling of cross-sections (**E**, **G**) and flatmounts (**F/F'**, **H/H'**) with antibodies against RFP (Rlbp1:Tomato) and M opsin (medium-wavelength cone opsin) of center areas of Rlbp-Cre WT mice (**E**, **F**) and 3-month Rlbp-Cre:Dicer-cKO$_{MG}$ mice (**G**, **H**). Insets in **F** and **H** are shown in **F'** and **H'**. *Arrowheads* indicate areas with reduced and scattered M opsin expression. Values are expressed as mean ± SEM. Significant differences are indicated. *$P \leq 0.05$, Mann–Whitney *U* test. *Scale bars*: 50 µm (**E**, **G**, **F'**, **H'**) and 200 µm (**F**, **H**). Layer explanation is given in Figure 1.

negative influence of adjacent cKO RPE cells. Overall, the partial alteration of the RPE in the Rlbp-Dicer-cKO mouse very likely contributed to observed retinal (rod) degeneration.

Glast-Cre:Dicer-cKO Mice Display a Similar Disease Phenotype But With More Persevered Retinal Structure

To assess the extent of RPE contribution to the observed phenotype in the Rlbp-Cre:Dicer-cKO mouse, we created the Glast-Cre:Dicer-cKO$_{MG}$ mouse with no reporter expression in the RPE.[54] Glast (i.e., glutamate aspartate transporter, encoded by Slc1a3 and also known as EEAT1) is expressed in brain astrocytes[55] and MG. We used the same experimental paradigm and validated the reporter induction in 3-month-old mice (Supplementary Fig. S4). RPE and retinal astrocytes were reporter negative in agreement with previous reports.[29,54] Retinal cross-sections and flatmounts showed similar induction patterns in MG compared to Rlbp-Cre; however, the efficiency was quite heterogeneous and a little less efficient (Glast-Cre with 70%–90% vs. Rlbp-Cre with ~98% reporter$^+$ MG of total MG).

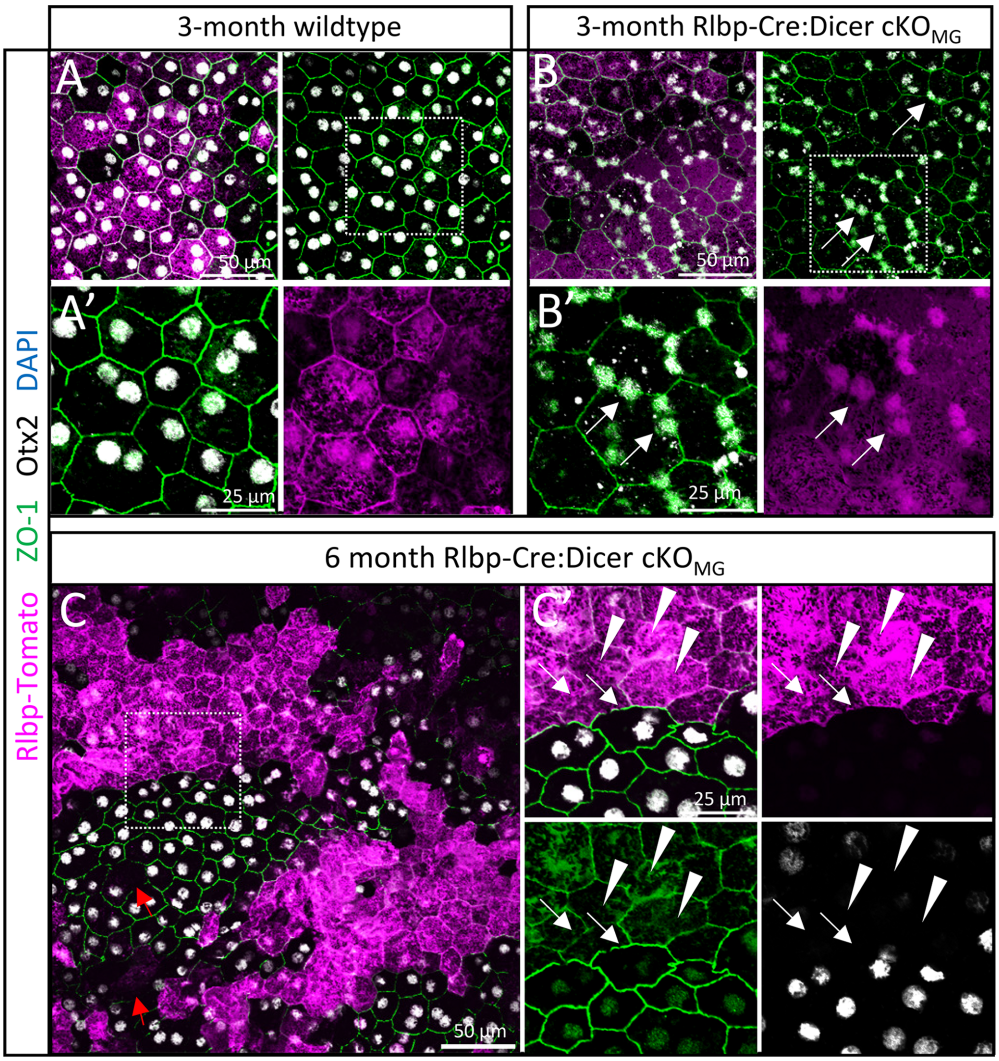

Figure 8. Rlbp-Cre:Dicer-cKO mice have partially impaired RPE. (**A–C**) Immunofluorescent labeling with antibodies against RFP (Rlbp1-Tomato), ZO-1, OTX2, and DAPI nuclear staining RPE flatmounts of 3-month Rlbp-Cre WT mice (**A**), 3-month Rlbp-Cre:Dicer-cKO mice (**B**), and 6-month Rlbp-Cre:Dicer-cKO mice (**C**). Insets in **A** to **C** are shown in **A'** to **C'**. *Arrows* in **B**/**B'** show altered nuclei locations in the 3-month Rlbp-Cre:Dicer-cKO mice. *Arrows* in **C'** show enlarged RPE cells or RPE cells that lost their ZO-1^{+} membrane. *Arrowheads* in **C'** show Rlbp-Cre:Dicer-cKO RPE cells with reduced ZO-1 and OTX2 expression. *Scale bars*: 50 µm (A–C) and 25 µm (**A'–C'**).

Next, we conducted OCT and ERG analysis of the Glast-CreER wildtype and cKO mice 3 and 6 months after Cre induction (Dicer deletion) to analyze structure and function (Fig. 9A). OCT scans showed that Glast-Cre wildtype mice were not different form Rlbp-Cre or any other wildtype strain. In the 3-month Glast-Cre:Dicer-cKO$_{MG}$ mice, the overall retinal architecture was normal but hyperreflective foci were present in the ELM–RPE region (Fig. 9B, arrowheads; Supplementary Figs. S5A–S5C). This finding suggests that these hyperreflective foci are primarily caused by MG dysfunction and not by RPE impairment. The retinas of 6-month Glast-Cre:Dicer-cKO$_{MG}$ mice were quite heterogeneous (probably due to less efficient induction), had thinner retinas than the wildtype retinas, and displayed more hyperreflective foci between the ELM and RPE compared to the Rlbp-Cre:Dicer-cKO$_{MG}$ retinas at this stage (Figs. 9D, 9E, arrowheads). This thinning was due to a reduction of the ELM–RPE area and the ONL, hence affecting photoreceptors. Overall, although the Rlbp-Dicer-cKO strain appeared more affected (ONL), both cKO strains resulted in similar thinning (Figs. 9E, 9F; Supplementary Figs. S5D, S5E).

Glast-Cre:Dicer-cKO Display Impaired Cone Function But More Preserved Rod Function

Because the first neuronal dysfunctions in the Rlbp-Cre:Dicer-cKO$_{MG}$ mouse concerned cones, we next conducted photopic ERG recordings in the Glast-Cre:Dicer-cKO$_{MG}$ mouse 3 and 6 months after Dicer deletion. Despite unaltered retinal structure, we found cone impairment 3 months after Dicer deletion, which further progressed over time (Figs. 10A, 10B). M opsin expression appeared scattered and fragmented, displaying the same phenotype as the Rlbp-Cre:Dicer-cKO$_{MG}$ mouse (Figs. 10C, 10D vs. Fig. 7). Because both MG Dicer-cKO$_{MG}$ strains resulted in the same outcome, the cone functional loss appears to be due to molecular (miRNA) alterations in MG.

Scotopic ERG recordings 3 and 4 months after Dicer deletion showed no rod photoreceptor impairment, in contrast

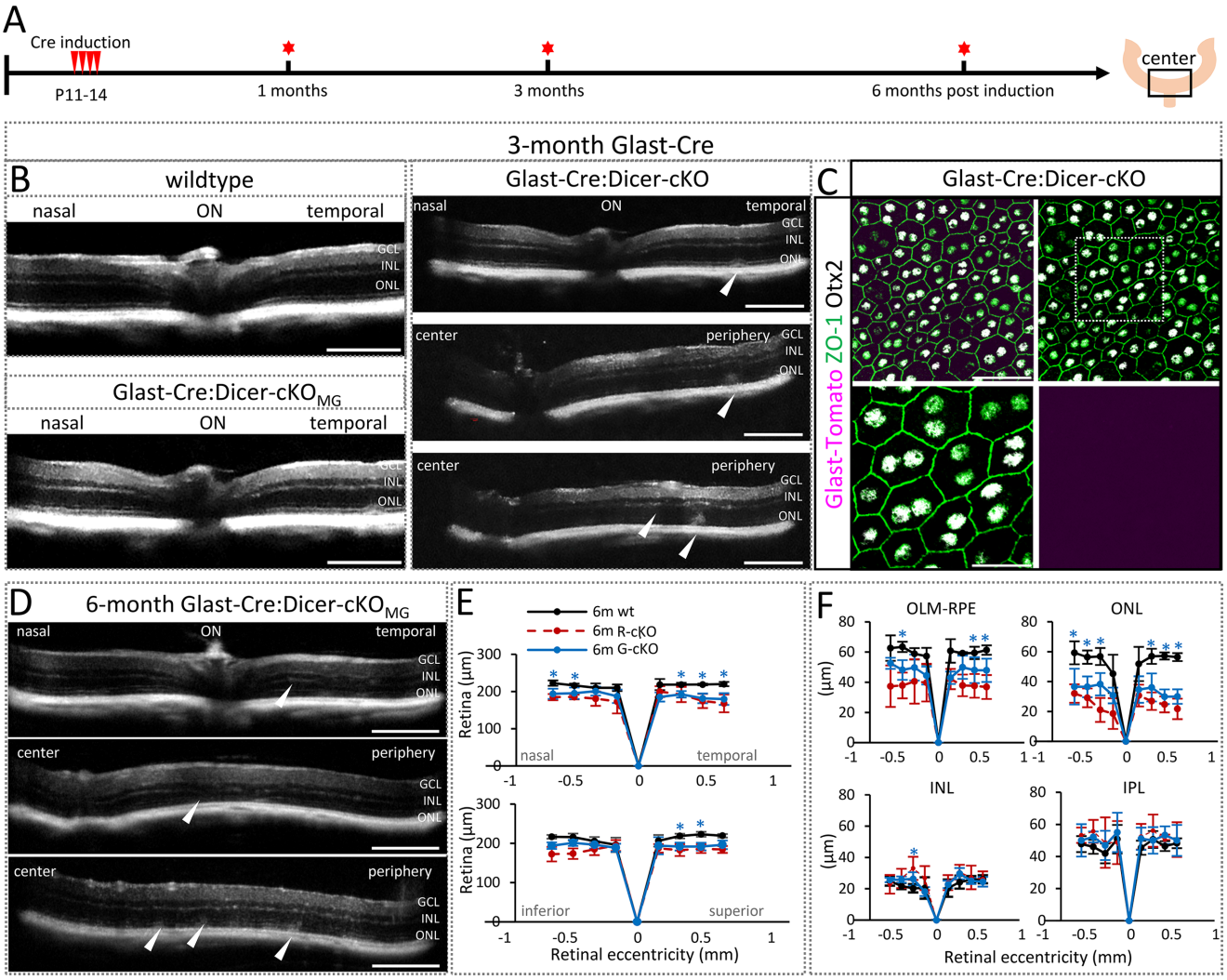

Figure 9. Glast-Cre:Dicer-cKO mice display hyperreflective foci and retinal thinning. (**A**) Experimental design. (**B**) OCT images of WT and or Glast-Cre:Dicer-cKO$_{MG}$ center at the nasal–temporal axis 3 months after Cre induction. (**C**) Immunofluorescent labeling of Glast-Cre:Dicer-cKO RPE flatmounts 3 months after Cre induction with antibodies against RFP (Glast:Tomato), ZO-1, OTX2, and DAPI. (**D**) OCT images of Glast-Cre:Dicer-cKO$_{MG}$ center at the nasal–temporal axis 6 months after Cre induction. *Arrowheads* in **B** and **D** indicate structural impairments. (**E**) Spider plots of the overall retinal thickness at the nasal–temporal and superior–inferior axis of WT mice (n = 5) and Glast-Cre:Dicer-cKO$_{MG}$ mice (n = 6) 6 months after Cre induction, in comparison to age-matched Rlbp-Cre:Dicer-cKO$_{MG}$ mice (n = 7). (**F**) Spider plots of the thickness (µm) of the retinal layers for WT and Glast-Cre:Dicer-cKO$_{MG}$ mice, in comparison to Rlbp-Cre:Dicer-cKO$_{MG}$ mice. Values are expressed as mean ± SD. Significant differences are indicated. *Wildtype-cKO comparison, +cKO-cKO comparison: $P \leq 0.05$, Mann–Whitney U test. *Scale bars*: 200 µm (**B**–**D**) and 25 µm (inset). Layer explanation is given in Figure 1.

to the observations in the Rlbp-Cre:Dicer-cKO$_{MG}$ mouse (Supplementary Figs. S6A, S6B). Naka–Rushton analysis also showed no alterations except an increased V_{max} (responsiveness) in the 4-month Glast-Cre:Dicer-cKO$_{MG}$ mouse compared to the wildtype. As mentioned before, a similar trend was seen in the Rlbp-Cre:Dicer-cKO$_{MG}$ mouse (Supplementary Fig. S6B vs. Fig. S63E).

Six-month Glast-Cre:Dicer-cKO$_{MG}$ retinas displayed rod dysfunction (scotopic a-wave) leading also to initial functional loss in the inner retina (scotopic b-wave) (Fig. 10E, Supplementary Figs. S6C). Overall, the scotopic functional loss in the 6-month Glast-Cre:Dicer-cKO$_{MG}$ mouse resembled the functional loss found in the 6-month Rlbp-Cre:Dicer-cKO$_{MG}$ mouse. However, the inner retina (rod bipolar cells) in the 6-month Glast-Cre:Dicer-cKO$_{MG}$ were less affected (unchanged V_{max}) (Supplementary Fig. S6C). Histological analysis showed that Glast-Cre:Dicer-cKO$_{MG}$ retinas also had areas with massive photoreceptor loss and ELM impairments (Figs. 10F–10H, arrows). In addition, MG in the 6-month Glast-Dicer-cKO$_{MG}$ had reduced or absent glutamine synthetase labeling (Figs. 10F', arrowheads).

Discussion

Many retinal dystrophies are not yet fully understood. Although retinitis pigmentosa or macular degenerations have predominantly genetic causes primarily affecting the RPE and photoreceptors, there is growing evidence that MG not only are responders to tissue changes but also contribute to disease progression[56–61] or might even participate in the initiation of degenerative events.[19,20,62–64]

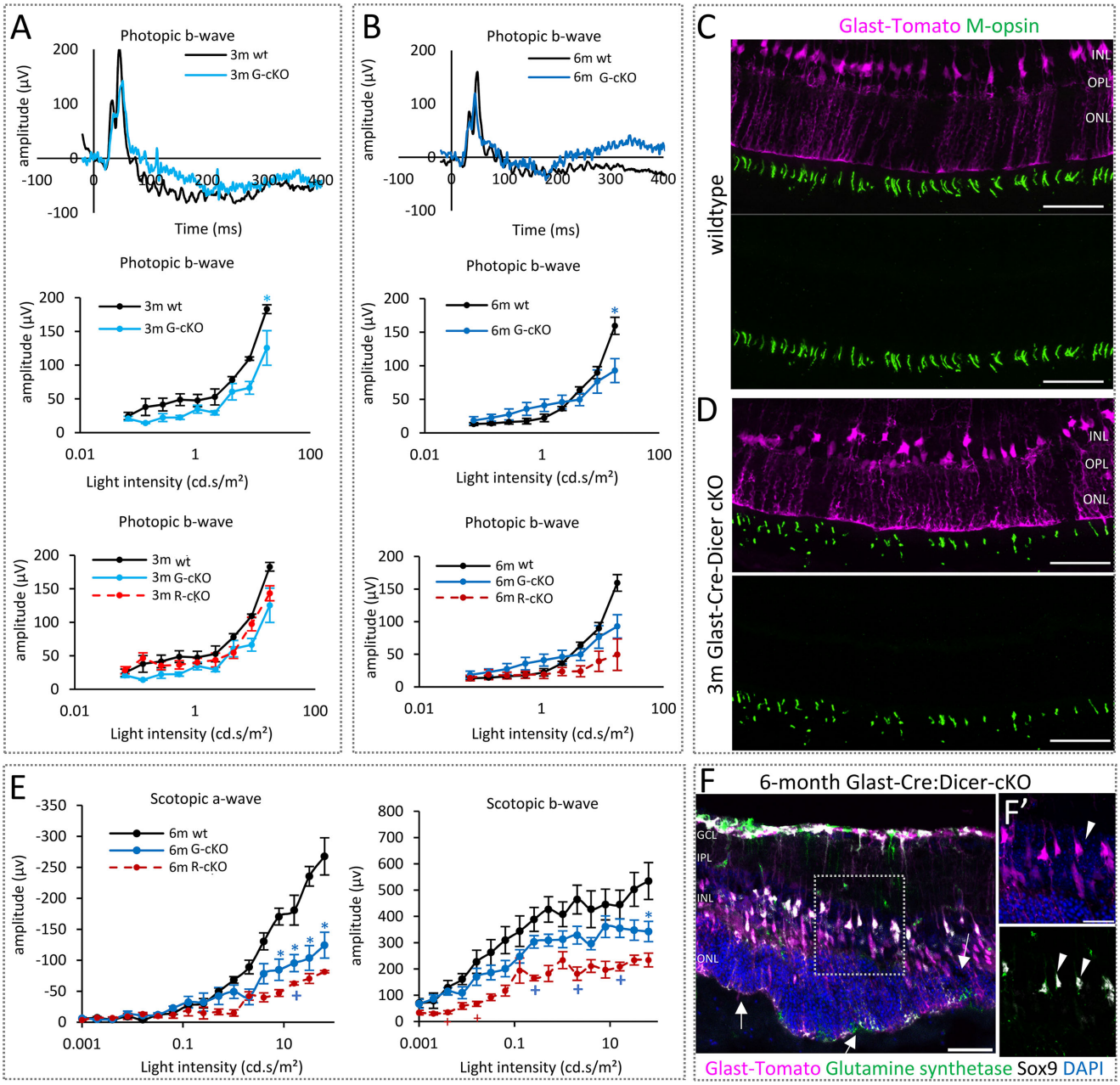

Figure 10. Glast-Cre:Dicer-cKO mice show loss of cone function 3 months after Dicer deletion. (**A**, **B**) Fullfield photopic ERG recordings showing representative ERG waveforms and b-wave intensity–amplitude plots of 3-month Glast-Cre:Dicer-cKO$_{MG}$ mice ($n = 5$) in comparison to WT mice ($n = 5$) (**A**) and 6-month Glast-Cre:Dicer-cKO$_{MG}$ mice ($n = 6$) in comparison to WT mice ($n = 5$) (**B**). (**C**, **D**) Immunofluorescent labeling of retinal cross-sections with antibodies against RFP (Glast:tdTomato) and M opsin (medium-wavelength cone opsin) of center areas of WT mice (**C**) and 3-month Glast-Cre:Dicer-cKO$_{MG}$ mice (**D**). (**E**) Fullfield scotopic ERG recordings showing a-wave and b-wave amplitudes of Glast-Cre:Dicer-cKO$_{MG}$ ($n = 6$) in comparison to WT ($n = 5$) and Rlbp-Cre:Dicer-cKO$_{MG}$ ($n = 5$). (**F**, **F'**) Immunofluorescent labeling of central retinal areas of the Glast-Cre:Dicer-cKO$_{MG}$ mouse 6 months after Dicer deletion, with antibodies against RFP (Glast:Tomato), GS, and SOX9, as well as DAPI nuclear staining. *Arrows* in **F** show a disturbed ELM, *arrowheads* in **F'** display GS-reduced MG. *Scale bars*: 50 µm (**C**, **D**, **F**) and 25 µm (**F'**). Values are expressed as mean ± SEM. Significant differences are indicated. *WT-cKO comparison, +cKO-cKO comparison: $P \leq 0.05$, Mann–Whitney *U* test. Layer explanation is given in Figure 1.

MG have a specific set of miRNAs different from those of neurons.[29] The loss of these MG-specific miRNAs in young glia results in abnormal glial behavior and a slow but severe photoceptor loss with subsequent retinal remodeling,[9] as it occurs in RP or AMD.[46,65–68] Therefore, any pathologies seen after manipulation are caused by malfunctioning MG, making this mouse a very interesting model for studying MG-induced retinal disease phenotypes. The onset and the order of events of the observed neurodegeneration, as well as whether the RPE contributes to the phenotype, were not known and were investigated in this study.

Here, we have shown that MG dysfunction, caused by the deletion of Dicer and mature miRNAs in the glia, leads first to impairments of cone health (summarized in Fig. 11).

Investigative Ophthalmology & Visual Science

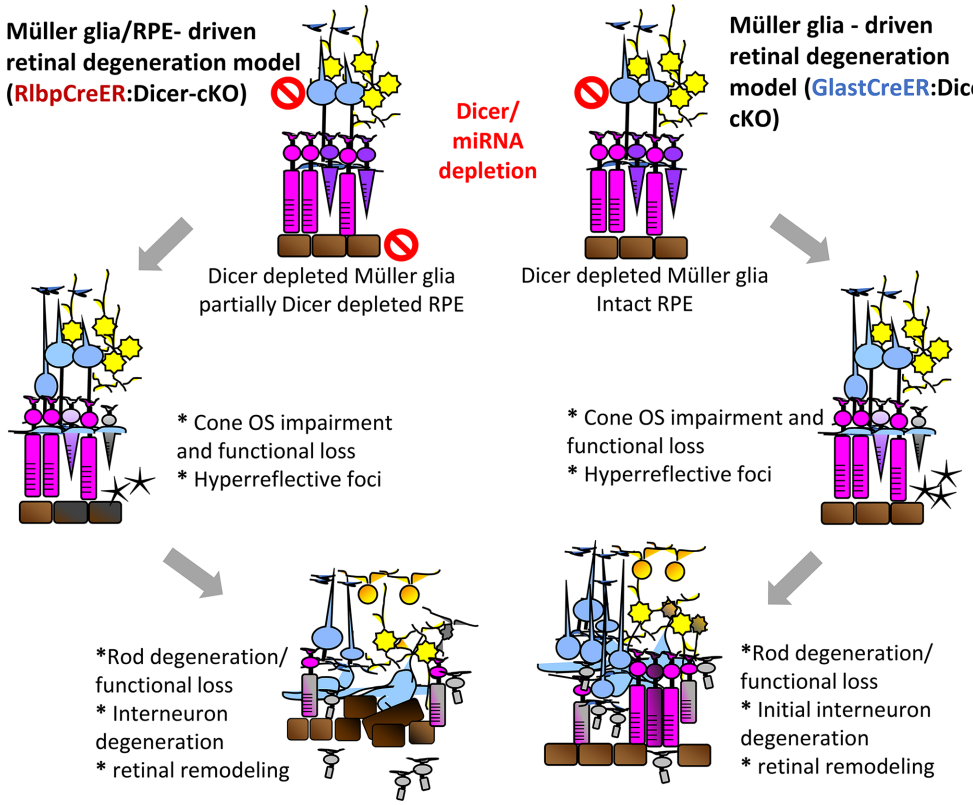

Figure 11. Dicer-depleted MG lead to cone functional loss with subsequent rod loss. Schematic overview of the major events happening in the MG/RPE-driven retinal degeneration model (Rlbp-CreER:Dicer-cKO) and the MG-driven retinal degeneration model (Glast-CreER:Dicer-cKO) emphasizing the shared pathological features: cone outer segment impairment and cone functional loss and hyperreflective foci in the ELM–RPE at the intermediate state and rod degeneration/rod functional loss and interneuron degeneration leading to retinal remodeling at the late stage. Additional features evident in both models include ELM breakage and glial seal formation. The Rlbp-CreER:Dicer-cKO model displayed furthermore impaired RPE contributing to rod loss and accelerating the overall pathological phenotype.

The first pathological indications are found in the ELM–RPE area. Structural and functional cone impairment was evident in two different MG reporter lines (i.e. Rlbp-Cre or Glast-Cre), 3 months after manipulation, validating this robust phenotype. Retinas of both strains displayed hyperreflective foci, which are considered indicators for disease,[69] in particular in AMD attributed to ectopic RPE.[70–72] Our Dicer-cKO model now suggests that hyperreflective foci can also be attributed to MG malfunction. Furthermore, cone impairment was followed by rod impairment, which was more accelerated in the Rlbp-Cre–driven strain, due to partial RPE malfunction. Therefore, the Glast-Cre strain allows the study of MG-driven events, and the Rlbp-Cre strain additionally allows the study of RPE-related events and RPE–MG interactions.

First Pathological Indications After Conditional Loss of Dicer and Mature miRNAs in MG Are Found in the ELM–RPE

As early as 1 month after Dicer deletion, we found a thicker ELM–RPE. The ELM, formed by tight and adherens junctions of MG and photoreceptors, plays a substantial role in disease manifestation and progression. An intact ELM is a requirement for an intact ellipsoid zone, and the integrity of both structures is vital for the preservation of normal vision. The ELM represents a barrier for macromolecules and is a structure formed by junctional complexes between inner photoreceptor segments and the outer processes of MG.[73–76] Alterations in the ELM with subsequent changes in the ellipsoid zone have been reported in diabetic retinopathy[77–81] and Stargardt disease.[61,82,83] With regard to diabetic retinopathy characterized by diabetic macular edema, it was reported that MG undergo hypertrophy. Their swollen endfeet lose their connection to the photoreceptors inner segments due to a decline in occludin,[76] a transmembrane protein that contributes to tight junction stabilization and optimal barrier function.[84] This disruption then leads to the accumulation of intraretinal fluid, primarily in the inner and outer plexiform layers, and manifests as retinal thickening and hyperreflective loci.

Furthermore, it is suggested that vascular endothelial growth factor (VEGF) alters tight junctions and promotes vascular permeability in the central nervous system, including the neural retina. Although the mechanisms of this barrier regulation are not yet fully understood, it was reported that VEGF induces phosphorylation-dependent occludin ubiquitination, which is necessary for increased permeability to macromolecules and ions.[85] MG are known to express VEGF[86,87] and therefore have been suspected of contributing to manifestation of the events seen in diabetic retinopathy.[88–90] The suspicion that MG are one of or even the driving components in these diseases was confirmed by MG ablation studies. The partial elimination (absence) of MG resulted in the same pathophysiological events.[19,20] In our

study, which is solely based on Dicer deletion with subsequent mature miRNAs depletion in the glia, we found these hallmarks suggesting that MG miRNAs might regulate these events. It was shown that miRNAs that directly target VEGF (3′UTR) include miR-16, miR-20a, miR-29b, miR-125, miR15c, and miR-200c,[91–96] and some of them are expressed in MG.[29]

Moreover, MG have been shown to actively contribute to absorbing excess fluid from the subretinal space via the water pore aquaporin-4 (AQP-4).[97,98] Two miRNAs, miR-29b and miR-320a, were identified as AQP-4 suppressors. miR-29 was found downregulated after stroke/cerebral ischemia, and its overexpression reduced the disruption of the blood–brain barrier after ischemic stroke by downregulating AQP-4.[99] Similarly, overexpression of miR-320a in the retina resulted in AQP-4 downregulation and attenuated hypoxia-induced injury including retinal edema.[100] A compromised MG function due to miRNA depletion might also cause an alteration in aquaporin expression causing liquid accumulation.

As mentioned before, ELM disruption can lead to fluid accumulation resulting in retinal thickening and hyperreflective loci. In our two independent MG Dicer cKO models (Rlbp-Cre and Glast-Cre), we found hyperreflective foci in the ELM–RPE area 3 months after Dicer/miRNA depletion. Hyperreflective foci belong to pathological features found in diabetic retinopathy/diabetic macular edema,[42] RP,[43–45] Stargardt disease,[61,82,83] and macular telangiectasia[101] and are a consequence of ELM impairment. Hyperreflective foci can also be detected in AMD, where they represent deposits rather than edema.[70,102,103] Because these foci were found in both of our cKO models (Rlbp-Cre and Glast-Cre), it stands to reason that they are predominantly a consequence of MG malfunction and less due to RPE malfunction. This conclusion is in agreement with two previous independent MG ablation studies in which the RPE was not affected.[19,20] This finding suggests that some retinal dystrophies and degenerative diseases, in particular the ones with unknown (non-genetic) origin, might be caused by imbalanced MG miRNAs. Furthermore, the fact that the same pathophysiological ELM–ellipsoid zone alterations were seen in animal models of retinal dystrophies[45,104] and ischemia,[105] which are models in in which solely neurons are targeted, further supports the hypothesis that the driving forces for these events are the glia.

A Decline in Cone Photoreceptor Function Precedes Rod Dysfunction

Müller glia have myriad functions in the healthy retina, one of which is cone pigment recycling.[18,106–109] We found impaired cone photoreceptor structure and function in both MG-specific Dicer-cKO strains, suggesting a central role for MG miRNAs in maintaining cone health in the retina. Cones are the photoreceptors involved in daylight and color vision, and maintaining cone health is crucial to maintaining proper visual function. Loss of cones and cone function is a feature of some retinal diseases such as AMD,[110,111] Leber's congenital amaurosis,[112,116] and Stargardt disease.[61,113,114] The cell type predominantly driving the retinal visual cycle is the MG.[107,115] MG generate 11-*cis*-retinol from the all-*trans* form via the enzyme cellular retinaldehyde binding protein (CRALBP), encoded by Rlbp1.[116–119] Hence, MG play a substantial role in visual pigment regeneration. Although the direct link between MG miRNAs and cone function in this model remains unknown and requires a subsequent investigation, it has been shown that loss or reduction of CRALBP expression in MG results in dislocated M opsin and reduced cone function.[109,120] Furthermore, it has been shown that peripheral regions in the RD1 retinitis pigmentosa mouse model harbor functional cones and that their prolonged survival is ensured by retinoic acid signaling of peripheral MG.[121] This suggests that MG miRNAs might play a role in regulating the MG-driven visual cycle.

Dicer/miRNA Loss in MG Leads to Rod Loss, With Partial Dicer Deletion in the RPE Accelerating the Process

Both MG-specific Dicer cKO strains resulted in rod loss accompanied by functional impairments that later on affected the inner retina. The overall progression of rod loss was very slow, but the pattern resembled the events found in rodent models of RP[122–124] and in the early stages of human forms of RP[125] caused by genetic defects. This suggests not only that MG contribute to the retinitis pigmentosa phenotype but also that MG miRNAs seem to regulate their behavior. Furthermore, we here utilized the Naka–Rushton equation, an analysis predominantly performed on patient ERGs, that allows an in-depth analysis of the b-wave with regard to responsiveness (V_{max}), sensitivity (K), and heterogeneity (slope n).[39–41] Overall, our Dicer-cKOs displayed similarities comparable to observations made in patient ERGs.[125] These similarities include a change in slope at early stages indicative for a patchy onset of functional loss.[40,41] This is followed by a reduction in responsiveness of rod bipolar cells due to a reduced rod input[126] but the sensitivity (basically the function of the cells) is stable during the intermediate phase (4 months). Finally, at the late stage (6 months), rod bipolar cells display a reduced responsiveness and a decline in sensitivity associated with retinal remodeling, affecting all inner neurons as it occurs at late stages of disease.[30,46–48] The similarities between these disease studies and our model suggest that, in addition to direct damage to photoreceptors or RPE, as occurs in many inherited RP forms, impaired or malfunctioning MG are very likely contributing substantially to the overall disease progression. More importantly, we showed that these pathological events were not caused by MG absence[19,20] but rather miRNA imbalances in the glia.

However, although cone impairments occurred at the same stage after Dicer loss, the rod loss was more accelerated in the Rlbp-Cre–driven strain that had a partially impaired RPE. The RPE has a variety of pivotal functions required for photoreceptor health and overall retinal health, including continuous renewal of the photoreceptor outer segments, isomerization of all-*trans*-retinal to 11-*cis*-retinal, and formation of the blood–retinal barrier.[127–129] Because of all these vital functions, impairment of the RPE not only accompanies but can also lead to photoreceptor degeneration.[3,128,130,131]

Because miRNAs play a significant role in regulating essential biological processes by targeting networks of functionally correlated genes, they are vital components of the molecular networks in the RPE.[132,133] In fact, RPE Dicer-cKO studies, as well as studies on selected miRNAs, have shown that RPE miRNAs are required for proper RPE maturation and function.[6,7,10,130,134–139]

Investigative Ophthalmology & Visual Science

In the Rlbp-Dicer-cKO, we found obvious changes in Dicer miRNA-deprived RPE, including disrupted expression of ZO-1, dislocation of RPE nuclei, and enlarged cell size. Altered ZO-1 expression and enlarged cell size are a known pathophysiological feature indicating RPE malfunction.[140–143] More importantly, drastically altered ZO-1 expression has been reported after Dicer deletion,[7,10] as well as after DiGeorge syndrome chromosomal region 8 (DGCR8) deletion, confirming that not just Dicer loss per se but also miRNA can cause RPE alteration.[7] DGCR8 is a part of the Drosha complex that generates precursor miRNAs from primary miRNA transcripts. This study also showed that the observed alterations were due to miRNA loss and not due to *Alu* element accumulations, which are known to contribute to photoreceptor loss in AMD.[7,144] Because *Alu* elements were also absent in the datasets obtained from FACS-purified MG from the Rlbp-CreER:Dicer-cKO$_{MG}$ mice, it is rather unlikely that they play a substantial role in the observed phenotypes.[9,21]

Together, our data show that dysregulated but physically still present MG lead to cone impairment in an otherwise healthy retina. This suggests an additional or even new prospect for the development of retinal diseases, particularly cone dystrophies of unknown origin. Furthermore, our findings indicate that drastic molecular changes long precede histological and functional changes. Histological manifestation (clinical observation) occurs relatively late, which might be the reason for difficulties in treating such complex diseases.

Acknowledgments

The authors thank Monica Andrade for her assistance with this study.

Supported by a grant from the New York Empire Innovation Program (SGW); grants from the National Eye Institute, National Institutes of Health (R01 EY032532 to SGW; R01 EY024373 and R21 EY032724 to SF); SUNY Startup Funds (SGW); SUNY Graduate Assistantship (DL, SK, SC); National Eye Institute T35 award (AMR); Catalyst Award from Research to Prevent Blindness Inc./American Macular Degeneration Foundation, an unrestricted award to the Department of Ophthalmology and Visual Sciences at Vanderbilt University Medical Center from Research to Prevent Blindness, Inc. (SF).

Disclosure: **D. Larbi**, None; **A.M. Rief**, None; **S. Kang**, None; **S. Chen**, None; **K. Batsuuri**, None; **S. Fuhrmann**, None; **S. Viswanathan**, None; **S.G. Wohl**, None

References

1. Barnstable CJ. Epigenetics and degenerative retinal diseases: prospects for new therapeutic approaches. *Asia Pac J Ophthalmol (Phila)*. 2022;11:328–334.
2. Zuzic M, Rojo Arias JE, Wohl SG, Busskamp V. Retinal miRNA functions in health and disease. *Genes (Basel)*. 2019;10:377.
3. Intartaglia D, Giamundo G, Conte I. The impact of miRNAs in health and disease of retinal pigment epithelium. *Front Cell Dev Biol*. 2020;8:589985.
4. Sun LF, Chen XJ, Jin ZB. Emerging roles of non-coding RNAs in retinal diseases: a review. *Clin Exp Ophthalmol*. 2020;48:1085–1101.
5. Sundermeier TR, Palczewski K. The physiological impact of microRNA gene regulation in the retina. *Cell mol Life Sci*. 2012;69:2739–2750.
6. Sundermeier TR, Palczewski K. The impact of microRNA gene regulation on the survival and function of mature cell types in the eye. *FASEB J*. 2016;30:23–33.
7. Sundermeier TR, Sakami S, Sahu B, et al. MicroRNA-processing enzymes are essential for survival and function of mature retinal pigmented epithelial cells in mice. *J Biol Chem*. 2017;292:3366–3378.
8. Sundermeier TR, Zhang N, Vinberg F, et al. DICER1 is essential for survival of postmitotic rod photoreceptor cells in mice. *FASEB J*. 2014;28:3780–3791.
9. Wohl SG, Jorstad NL, Levine EM, Reh TA. Müller glial microRNAs are required for the maintenance of glial homeostasis and retinal architecture. *Nat Commun*. 2017;8:1603.
10. Wright CB, Uehara H, Kim Y, et al. Chronic Dicer1 deficiency promotes atrophic and neovascular outer retinal pathologies in mice. *Proc Natl Acad Sci USA*. 2020;117:2579–2587.
11. Bringmann A, Pannicke T, Grosche J, et al. Müller cells in the healthy and diseased retina. *Prog Retin Eye Res*. 2006;25:397–424.
12. Bringmann A, Francke M, Pannicke T, et al. Role of glial K^+ channels in ontogeny and gliosis: a hypothesis based upon studies on Müller cells. *Glia*. 2000;29:35–44.
13. Bringmann A, Reichenbach A. Role of Müller cells in retinal degenerations. *Front Biosci*. 2001;6:E72–E92.
14. Kuhrt H, Wurm A, Karl A, et al. Müller cell gliosis in retinal organ culture mimics gliotic alterations after ischemia in vivo. *Int J Dev Neurosci*. 2008;26:745–751.
15. Newman E, Reichenbach A. The Müller cell: a functional element of the retina. *Trends Neurosci*. 1996;19:307–312.
16. Reichenbach A, Bringmann A. New functions of Müller cells. *Glia*. 2013;61:651–678.
17. Reichenbach A, Stolzenburg JU, Eberhardt W, Chao TI, Dettmer D, Hertz L. What do retinal Müller (glial) cells do for their neuronal 'small siblings'? *J Chem Neuroanat*. 1993;6:201–213.
18. Wang JS, Kefalov VJ. The cone-specific visual cycle. *Prog Retin Eye Res*. 2011;30:115–128.
19. Byrne LC, Khalid F, Lee T, et al. AAV-mediated, optogenetic ablation of Müller glia leads to structural and functional changes in the mouse retina. *PLoS One*. 2013;8:e76075.
20. Shen W, Fruttiger M, Zhu L, et al. Conditional Müller cell ablation causes independent neuronal and vascular pathologies in a novel transgenic model. *J Neurosci*. 2012;32:15715–15727.
21. Kang S, Larbi D, Andrade M, Reardon S, Reh TA, Wohl SG. A comparative analysis of reactive Müller glia gene expression after light damage and microRNA-depleted Müller glia—focus on microRNAs. *Front Cell Dev Biol*. 2020;8:620459.
22. Vazquez-Chona FR, Clark AM, Levine EM. Rlbp1 promoter drives robust Müller glial GFP expression in transgenic mice. *Invest Ophthalmol Vis Sci*. 2009;50:3996–4003.
23. Harfe BD, McManus MT, Mansfield JH, Hornstein E, Tabin CJ. The RNaseIII enzyme Dicer is required for morphogenesis but not patterning of the vertebrate limb. *Proc Natl Acad Sci USA*. 2005;102:10898–10903.
24. Wong RL, Lee JW, Yau GS, Wong IY. Relationship between outer retinal layers thickness and visual acuity in diabetic macular edema. *Biomed Res Int*. 2015;2015:981471.
25. Li Y, Zhang Y, Chen S, Vernon G, Wong WT, Qian H. Light-dependent OCT structure changes in photoreceptor degenerative rd 10 mouse retina. *Invest Ophthalmol Vis Sci*. 2018;59:1084–1094.
26. Severns ML, Johnson MA. The care and fitting of Naka–Rushton functions to electroretinographic intensity-response data. *Doc Ophthalmol*. 1993;85:135–150.

Investigative Ophthalmology & Visual Science

27. Evans LS, Peachey NS, Marchese AL. Comparison of three methods of estimating the parameters of the Naka–Rushton equation. *Doc Ophthalmol*. 1993;84:19–30.
28. Claybon A, Bishop AJ. Dissection of a mouse eye for a whole mount of the retinal pigment epithelium. *J Vis Exp*. 2011;48:2563.
29. Wohl SG, Reh TA. The microRNA expression profile of mouse Müller glia in vivo and in vitro. *Sci Rep*. 2016;6:35423.
30. Marc RE, Jones BW. Retinal remodeling in inherited photoreceptor degenerations. *Mol Neurobiol*. 2003;28:139–147.
31. Kalloniatis M, Nivison-Smith L, Chua J, Acosta ML, Fletcher EL. Using the rd1 mouse to understand functional and anatomical retinal remodelling and treatment implications in retinitis pigmentosa: a review. *Exp Eye Res*. 2016;150:106–121.
32. Chiba C. The retinal pigment epithelium: an important player of retinal disorders and regeneration. *Exp Eye Res*. 2014;123:107–114.
33. Pennesi ME, Michaels KV, Magee SS, et al. Long-term characterization of retinal degeneration in rd1 and rd10 mice using spectral domain optical coherence tomography. *Invest Ophthalmol Vis Sci*. 2012;53:4644–4656.
34. Ferreira H, Martins J, Moreira PI, et al. Longitudinal normative OCT retinal thickness data for wild-type mice, and characterization of changes in the 3xTg-AD mice model of Alzheimer's disease. *Aging (Albany NY)*. 2021;13:9433–9454.
35. Ferguson LR, Grover S, Dominguez JM, 2nd, Balaiya S, Chalam KV. Retinal thickness measurement obtained with spectral domain optical coherence tomography assisted optical biopsy accurately correlates with ex vivo histology. *PLoS One*. 2014;9:e111203.
36. Aleman TS, Cideciyan AV, Sumaroka A, et al. Retinal laminar architecture in human retinitis pigmentosa caused by Rhodopsin gene mutations. *Invest Ophthalmol Vis Sci*. 2008;49:1580–1590.
37. Sayo A, Ueno S, Kominami T, et al. Significant relationship of visual field sensitivity in central 10 degrees to thickness of retinal layers in retinitis pigmentosa. *Invest Ophthalmol Vis Sci*. 2018;59:3469–3475.
38. Yavuzer K, Citirik M, Yavuzer B. Evaluation of structural retinal layer alterations in retinitis pigmentosa. *Rom J Ophthalmol*. 2023;67:326–336.
39. Naka KI, Rushton WA. S-potentials from colour units in the retina of fish (Cyprinidae). *J Physiol*. 1966;185:536–555.
40. Massof RW, Wu L, Finkelstein D, Perry C, Starr SJ, Johnson MA. Properties of electroretinographic intensity-response functions in retinitis pigmentosa. *Doc Ophthalmol*. 1984;57:279–296.
41. Peachey NS, Fishman GA, Derlacki DJ, Alexander KR. Rod and cone dysfunction in carriers of X-linked retinitis pigmentosa. *Ophthalmology*. 1988;95:677–685.
42. Uji A, Murakami T, Nishijima K, et al. Association between hyperreflective foci in the outer retina, status of photoreceptor layer, and visual acuity in diabetic macular edema. *Am J Ophthalmol*. 2012;153:710–717, 717.e1.
43. Hamada S, Yoshida K, Chihara E. Optical coherence tomography images of retinitis pigmentosa. *Ophthalmic Surg Lasers*. 2000;31:253–256.
44. Hanumunthadu D, Rasheed MA, Goud A, Gupta A, Vupparaboina KK, Chhablani J. Choroidal hyper-reflective foci and vascularity in retinal dystrophy. *Indian J Ophthalmol*. 2020;68:130–133.
45. Nakazawa M, Hara A, Ishiguro SI. Optical coherence tomography of animal models of retinitis pigmentosa: from animal studies to clinical applications. *Biomed Res Int*. 2019;2019:8276140.
46. Jones BW, Marc RE. Retinal remodeling during retinal degeneration. *Exp Eye Res*. 2005;81:123–137.
47. Jones BW, Pfeiffer RL, Ferrell WD, Watt CB, Marmor M, Marc RE. Retinal remodeling in human retinitis pigmentosa. *Exp Eye Res*. 2016;150:149–165.
48. Jones BW, Watt CB, Frederick JM, et al. Retinal remodeling triggered by photoreceptor degenerations. *J Comp Neurol*. 2003;464:1–16.
49. Brandli A, Stone J. Using the electroretinogram to assess function in the rodent retina and the protective effects of remote limb ischemic preconditioning. *J Vis Exp*. 2015;100:e52658.
50. Lyubarsky AL, Lem J, Chen J, Falsini B, Iannaccone A, Pugh EN, Jr. Functionally rodless mice: transgenic models for the investigation of cone function in retinal disease and therapy. *Vision Res*. 2002;42:401–415.
51. Konari K, Sawada N, Zhong Y, Isomura H, Nakagawa T, Mori M. Development of the blood–retinal barrier in vitro: formation of tight junctions as revealed by occludin and ZO-1 correlates with the barrier function of chick retinal pigment epithelial cells. *Exp Eye Res*. 1995;61:99–108.
52. Martinez-Morales JR, Dolez V, Rodrigo I, et al. OTX2 activates the molecular network underlying retina pigment epithelium differentiation. *J Biol Chem*. 2003;278:21721–21731.
53. Nishihara D, Yajima I, Tabata H, et al. Otx2 is involved in the regional specification of the developing retinal pigment epithelium by preventing the expression of Sox2 and *Fgf8*, factors that induce neural retina differentiation. *PLoS One*. 2012;7:e48879.
54. Shao A, Lopez AJ, Chen J, et al. Arap1 loss causes retinal pigment epithelium phagocytic dysfunction and subsequent photoreceptor death. *Dis Model Mech*. 2022;15:dmm049343.
55. Slezak M, Goritz C, Niemiec A, et al. Transgenic mice for conditional gene manipulation in astroglial cells. *Glia*. 2007;55:1565–1576.
56. Bhutto IA, Ogura S, Baldeosingh R, McLeod DS, Lutty GA, Edwards MM. An acute injury model for the phenotypic characteristics of geographic atrophy. *Invest Ophthalmol Vis Sci*. 2018;59:AMD143–AMD151.
57. Edwards MM, McLeod DS, Bhutto IA, Grebe R, Duffy M, Lutty GA. Subretinal glial membranes in eyes with geographic atrophy. *Invest Ophthalmol Vis Sci*. 2017;58:1352–1367.
58. Wu KH, Madigan MC, Billson FA, Penfold PL. Differential expression of GFAP in early v late AMD: a quantitative analysis. *Br J Ophthalmol*. 2003;87:1159–1166.
59. Edwards MM, McLeod DS, Shen M, et al. Clinicopathologic findings in three siblings with geographic atrophy. *Invest Ophthalmol Vis Sci*. 2023;64:2.
60. Edwards MM, McLeod DS, Bhutto IA, Villalonga MB, Seddon JM, Lutty GA. Idiopathic preretinal glia in aging and age-related macular degeneration. *Exp Eye Res*. 2016;150:44–61.
61. Sherman J. A novel biomarker for Stargardt disease? *Rev Optometry*. 2013;150:58–67.
62. Powner MB, Gillies MC, Zhu M, Vevis K, Hunyor AP, Fruttiger M. Loss of Müller's cells and photoreceptors in macular telangiectasia type 2. *Ophthalmology*. 2013;120:2344–2352.
63. Nash BM, Wright DC, Grigg JR, Bennetts B, Jamieson RV. Retinal dystrophies, genomic applications in diagnosis and prospects for therapy. *Transl Pediatr*. 2015;4:139–163.
64. Navneet S, Wilson K, Rohrer B. Müller glial cells in the macula: their activation and cell–cell interactions in age-related macular degeneration. *Invest Ophthalmol Vis Sci*. 2024;65:42.

Investigative Ophthalmology & Visual Science

65. Edwards MM, McLeod DS, Grebe R, et al. Glial remodeling and choroidal vascular pathology in eyes from two donors with choroideremia. *Front Ophthalmol (Lausanne)*. 2022;2:994566.
66. Curcio CA, Medeiros NE, Millican CL. Photoreceptor loss in age-related macular degeneration. *Invest Ophthalmol Vis Sci*. 1996;37:1236–1249.
67. Kinnunen K, Petrovski G, Moe MC, Berta A, Kaarniranta K. Molecular mechanisms of retinal pigment epithelium damage and development of age-related macular degeneration. *Acta Ophthalmol*. 2012;90:299–309.
68. Pfau M, von der Emde L, de Sisternes L, et al. Progression of photoreceptor degeneration in geographic atrophy secondary to age-related macular degeneration. *JAMA Ophthalmol*. 2020;138:1026–1034.
69. Fragiotta S, Abdolrahimzadeh S, Dolz-Marco R, Sakurada Y, Gal-Or O, Scuderi G. Significance of hyperreflective foci as an optical coherence tomography biomarker in retinal diseases: characterization and clinical implications. *J Ophthalmol*. 2021;2021:6096017.
70. Landa G, Rosen RB, Pilavas J, Garcia PM. Drusen characteristics revealed by spectral-domain optical coherence tomography and their corresponding fundus autofluorescence appearance in dry age-related macular degeneration. *Ophthalmic Res*. 2012;47:81–86.
71. Romano F, Ding X, Yuan M, et al. Progressive choriocapillaris changes on optical coherence tomography angiography correlate with stage progression in AMD. *Invest Ophthalmol Vis Sci*. 2024;65:21.
72. Cao D, Leong B, Messinger JD, et al. Hyperreflective foci, optical coherence tomography progression indicators in age-related macular degeneration, include transdifferentiated retinal pigment epithelium. *Invest Ophthalmol Vis Sci*. 2021;62:34.
73. Drexler W, Sattmann H, Hermann B, et al. Enhanced visualization of macular pathology with the use of ultrahigh-resolution optical coherence tomography. *Arch Ophthalmol*. 2003;121:695–706.
74. Srinivasan VJ, Monson BK, Wojtkowski M, et al. Characterization of outer retinal morphology with high-speed, ultrahigh-resolution optical coherence tomography. *Invest Ophthalmol Vis Sci*. 2008;49:1571–1579.
75. Zhang XL, Wen L, Chen YJ, Zhu Y. Vascular endothelial growth factor up-regulates the expression of intracellular adhesion molecule-1 in retinal endothelial cells via reactive oxygen species, but not nitric oxide. *Chin Med J (Engl)*. 2009;122:338–343.
76. Omri S, Omri B, Savoldelli M, et al. The outer limiting membrane (OLM) revisited: clinical implications. *Clin Ophthalmol*. 2010;4:183–195.
77. De S, Saxena S, Kaur A, et al. Sequential restoration of external limiting membrane and ellipsoid zone after intravitreal anti-VEGF therapy in diabetic macular oedema. *Eye (Lond)*. 2021;35:1490–1495.
78. Saxena S, Akduman L, Meyer CH. External limiting membrane: retinal structural barrier in diabetic macular edema. *Int J Retina Vitreous*. 2021;7:16.
79. Saxena S, Meyer CH, Akduman L. External limiting membrane and ellipsoid zone structural integrity in diabetic macular edema. *Eur J Ophthalmol*. 2022;32:15–16.
80. Saxena S, Sadda SR. Focus on external limiting membrane and ellipsoid zone in diabetic macular edema. *Indian J Ophthalmol*. 2021;69:2925–2927.
81. Chhablani JK, Kim JS, Cheng L, Kozak I, Freeman W. External limiting membrane as a predictor of visual improvement in diabetic macular edema after pars plana vitrectomy. *Graefes Arch Clin Exp Ophthalmol*. 2012;250:1415–1420.
82. Tanna P, Strauss RW, Fujinami K, Michaelides M. Stargardt disease: clinical features, molecular genetics, animal models and therapeutic options. *Br J Ophthalmol*. 2017;101:25–30.
83. Whitmore SS, Fortenbach CR, Cheng JL, et al. Analysis of retinal sublayer thicknesses and rates of change in *ABCA4*-associated Stargardt disease. *Sci Rep*. 2020;10:16576.
84. Cummins PM. Occludin: one protein, many forms. *Mol Cell Biol*. 2012;32:242–250.
85. Murakami T, Felinski EA, Antonetti DA. Occludin phosphorylation and ubiquitination regulate tight junction trafficking and vascular endothelial growth factor-induced permeability. *J Biol Chem*. 2009;284:21036–21046.
86. Pierce EA, Avery RL, Foley ED, Aiello LP, Smith LE. Vascular endothelial growth factor/vascular permeability factor expression in a mouse model of retinal neovascularization. *Proc Natl Acad Sci USA*. 1995;92:905–909.
87. Robbins SG, Conaway JR, Ford BL, Roberto KA, Penn JS. Detection of vascular endothelial growth factor (VEGF) protein in vascular and non-vascular cells of the normal and oxygen-injured rat retina. *Growth Factors*. 1997;14:229–241.
88. Bai Y, Ma JX, Guo J, et al. Müller cell-derived VEGF is a significant contributor to retinal neovascularization. *J Pathol*. 2009;219:446–454.
89. Wang J, Xu X, Elliott MH, Zhu M, Le YZ. Müller cell-derived VEGF is essential for diabetes-induced retinal inflammation and vascular leakage. *Diabetes*. 2010;59:2297–2305.
90. Le YZ. VEGF production and signaling in Müller glia are critical to modulating vascular function and neuronal integrity in diabetic retinopathy and hypoxic retinal vascular diseases. *Vision Res*. 2017;139:108–114.
91. Sun CY, She XM, Qin Y, et al. miR-15a and miR-16 affect the angiogenesis of multiple myeloma by targeting VEGF. *Carcinogenesis*. 2013;34:426–435.
92. Witvrouwen I, Mannaerts D, Ratajczak J, et al. MicroRNAs targeting VEGF are related to vascular dysfunction in preeclampsia. *Biosci Rep*. 2021;41:BSR20210874.
93. Wang Q, Navitskaya S, Chakravarthy H, et al. Dual anti-inflammatory and anti-angiogenic action of miR-15a in diabetic retinopathy. *EBioMedicine*. 2016;11:138–150.
94. Yang Y, Liu Y, Li Y, et al. MicroRNA-15b targets VEGF and inhibits angiogenesis in proliferative diabetic retinopathy. *J Clin Endocrinol Metab*. 2020;105:3404–3415.
95. Ye EA, Liu L, Steinle JJ. miR-15a/16 inhibits TGF-beta3/VEGF signaling and increases retinal endothelial cell barrier proteins. *Vision Res*. 2017;139:23–29.
96. Fan YC, Mei PJ, Chen C, Miao FA, Zhang H, Li ZL. MiR-29c inhibits glioma cell proliferation, migration, invasion and angiogenesis. *J Neurooncol*. 2013;115:179–188.
97. Nagelhus EA, Veruki ML, Torp R, et al. Aquaporin-4 water channel protein in the rat retina and optic nerve: polarized expression in Müller cells and fibrous astrocytes. *J Neurosci*. 1998;18:2506–2519.
98. Reichenbach A, Wurm A, Pannicke T, Iandiev I, Wiedemann P, Bringmann A. Müller cells as players in retinal degeneration and edema. *Graefes Arch Clin Exp Ophthalmol*. 2007;245:627–636.
99. Wang Y, Huang J, Ma Y, et al. MicroRNA-29b is a therapeutic target in cerebral ischemia associated with aquaporin 4. *J Cereb Blood Flow Metab*. 2015;35:1977–1984.
100. Chen Z, Yang Z, Li X, et al. microRNA-320a prevent Müller cells from hypoxia injury by targeting aquaporin-4. *J Cell Biochem*. 2020;121:4711–4723.
101. Pauleikhoff D, Bonelli R, Dubis AM, et al. Progression characteristics of ellipsoid zone loss in macular telangiectasia type 2. *Acta Ophthalmol*. 2019;97:e998–e1005.
102. Ferrara D, Silver RE, Louzada RN, Novais EA, Collins GK, Seddon JM. Optical coherence tomography features

Investigative Ophthalmology & Visual Science

preceding the onset of advanced age-related macular degeneration. *Invest Ophthalmol Vis Sci*. 2017;58:3519–3529.

103. Khanifar AA, Koreishi AF, Izatt JA, Toth CA. Drusen ultrastructure imaging with spectral domain optical coherence tomography in age-related macular degeneration. *Ophthalmology*. 2008;115:1883–1890.
104. Adachi K, Takahashi S, Yamauchi K, Mounai N, Tanabu R, Nakazawa M. Optical coherence tomography of retinal degeneration in Royal College of Surgeons rats and its correlation with morphology and electroretinography. *PLoS One*. 2016;11:e0162835.
105. Martinez-Gil N, Kutsyr O, Fernandez-Sanchez L, et al. Ischemia-reperfusion increases TRPM7 expression in mouse retinas. *Int J Mol Sci*. 2023;24:16068.
106. Fleisch VC, Schonthaler HB, von Lintig J, Neuhauss SC. Subfunctionalization of a retinoid-binding protein provides evidence for two parallel visual cycles in the cone-dominant zebrafish retina. *J Neurosci*. 2008;28:8208–8216.
107. Muniz A, Villazana-Espinoza ET, Thackeray B, Tsin AT. 11-*cis*-Acyl-CoA:retinol *O*-acyltransferase activity in the primary culture of chicken Müller cells. *Biochemistry*. 2006;45:12265–12273.
108. Rodgers HM, Huffman VJ, Voronina VA, Lewandoski M, Mathers PH. The role of the *Rx* homeobox gene in retinal progenitor proliferation and cell fate specification. *Mech Dev*. 2018;151:18–29.
109. Xue Y, Shen SQ, Jui J, et al. CRALBP supports the mammalian retinal visual cycle and cone vision. *J Clin Invest*. 2015;125:727–738.
110. Hogg RE, Chakravarthy U. Visual function and dysfunction in early and late age-related maculopathy. *Prog Retin Eye Res*. 2006;25:249–276.
111. Shelley EJ, Madigan MC, Natoli R, Penfold PL, Provis JM. Cone degeneration in aging and age-related macular degeneration. *Arch Ophthalmol*. 2009;127:483–492.
112. Pennesi ME, Stover NB, Stone EM, Chiang PW, Weleber RG. Residual electroretinograms in young Leber congenital amaurosis patients with mutations of *AIPL1*. *Invest Ophthalmol Vis Sci*. 2011;52:8166–8173.
113. Fujinami K, Lois N, Davidson AE, et al. A longitudinal study of Stargardt disease: clinical and electrophysiologic assessment, progression, and genotype correlations. *Am J Ophthalmol*. 2013;155:1075–1088.e13.
114. Kumaran N, Ripamonti C, Kalitzeos A, Rubin GS, Bainbridge JWB, Michaelides M. Severe loss of tritan color discrimination in *RPE65* associated Leber congenital amaurosis. *Invest Ophthalmol Vis Sci*. 2018;59:85–93.
115. Das SR, Bhardwaj N, Kjeldbye H, Gouras P. Müller cells of chicken retina synthesize 11-*cis*-retinol. *Biochem J*. 1992;285:907–913.
116. Mata NL, Radu RA, Clemmons RC, Travis GH. Isomerization and oxidation of vitamin a in cone-dominant retinas: a novel pathway for visual-pigment regeneration in daylight. *Neuron*. 2002;36:69–80.
117. Bok D, Ong DE, Chytil F. Immunocytochemical localization of cellular retinol binding protein in the rat retina. *Invest Ophthalmol Vis Sci*. 1984;25:877–883.
118. Bunt-Milam AH, Saari JC. Immunocytochemical localization of two retinoid-binding proteins in vertebrate retina. *J Cell Biol*. 1983;97:703–712.
119. Eisenfeld AJ, Bunt-Milam AH, Saari JC. Localization of retinoid-binding proteins in developing rat retina. *Exp Eye Res*. 1985;41:299–304.
120. Kolesnikov AV, Kiser PD, Palczewski K, Kefalov VJ. Function of mammalian M-cones depends on the level of CRALBP in Müller cells. *J Gen Physiol*. 2021;153:e202012675.
121. Amamoto R, Wallick GK, Cepko CL. Retinoic acid signaling mediates peripheral cone photoreceptor survival in a mouse model of retina degeneration. *eLife*. 2022;11:e76389.
122. Bush RA, Hawks KW, Sieving PA. Preservation of inner retinal responses in the aged Royal College of Surgeons rat. Evidence against glutamate excitotoxicity in photoreceptor degeneration. *Invest Ophthalmol Vis Sci*. 1995;36:2054–2062.
123. Machida S, Kondo M, Jamison JA, et al. P23H rhodopsin transgenic rat: correlation of retinal function with histopathology. *Invest Ophthalmol Vis Sci*. 2000;41:3200–3209.
124. Chang B, Hawes NL, Hurd RE, Davisson MT, Nusinowitz S, Heckenlively JR. Retinal degeneration mutants in the mouse. *Vision Res*. 2002;42:517–525.
125. Birch DG, Fish GE. Rod ERGs in retinitis pigmentosa and cone–rod degeneration. *Invest Ophthalmol Vis Sci*. 1987;28:140–150.
126. Perlman I. The electroretinogram: ERG. In: Kolb H, Fernandez E, Jones BW, Nelson R, eds. *Webvision: The Organization of the Retina and Visual System*. Salt Lake City, UT: University of Utah Health Sciences Center; 1995.
127. Mazzoni F, Safa H, Finnemann SC. Understanding photoreceptor outer segment phagocytosis: use and utility of RPE cells in culture. *Exp Eye Res*. 2014;126:51–60.
128. Strauss O. The retinal pigment epithelium in visual function. *Physiol Rev*. 2005;85:845–881.
129. Simo R, Villarroel M, Corraliza L, Hernandez C, Garcia-Ramirez M. The retinal pigment epithelium: something more than a constituent of the blood-retinal barrier—implications for the pathogenesis of diabetic retinopathy. *J Biomed Biotechnol*. 2010;2010:190724.
130. Amram B, Cohen-Tayar Y, David A, Ashery-Padan R. The retinal pigmented epithelium – from basic developmental biology research to translational approaches. *Int J Dev Biol*. 2017;61:225–234.
131. Fuhrmann S, Zou C, Levine EM. Retinal pigment epithelium development, plasticity, and tissue homeostasis. *Exp Eye Res*. 2014;123:141–150.
132. Soundara Pandi SP, Chen M, Guduric-Fuchs J, Xu H, Simpson DA. Extremely complex populations of small RNAs in the mouse retina and RPE/choroid. *Invest Ophthalmol Vis Sci*. 2013;54:8140–8151.
133. Greene WA, Muniz A, Plamper ML, Kaini RR, Wang HC. MicroRNA expression profiles of human iPS cells, retinal pigment epithelium derived from iPS, and fetal retinal pigment epithelium. *J Vis Exp*. 2014;88:e51589.
134. Davis N, Mor E, Ashery-Padan R. Roles for Dicer1 in the patterning and differentiation of the optic cup neuroepithelium. *Development*. 2011;138:127–138.
135. Ohana R, Weiman-Kelman B, Raviv S, et al. MicroRNAs are essential for differentiation of the retinal pigmented epithelium and maturation of adjacent photoreceptors. *Development*. 2015;142:2487–2498.
136. Adijanto J, Castorino JJ, Wang ZX, Maminishkis A, Grunwald GB, Philp NJ. Microphthalmia-associated transcription factor (MITF) promotes differentiation of human retinal pigment epithelium (RPE) by regulating microRNAs-204/211 expression. *J Biol Chem*. 2012;287:20491–20503.
137. Yao R, Yao X, Liu R, Peng J, Tian T. Glucose-induced microRNA-218 suppresses the proliferation and promotes the apoptosis of human retinal pigment epithelium cells by targeting RUNX2. *Biosci Rep*. 2019;39:BSR20192580.
138. Jiang C, Qin B, Liu G, et al. MicroRNA-184 promotes differentiation of the retinal pigment epithelium by

Investigative Ophthalmology & Visual Science

targeting the AKT2/mTOR signaling pathway. *Oncotarget*. 2016;7:52340–52353.

139. Shao Y, Dong LJ, Takahashi Y, et al. miRNA-451a regulates RPE function through promoting mitochondrial function in proliferative diabetic retinopathy. *Am J Physiol Endocrinol Metab*. 2019;316:E443–E452.
140. Bailey TA, Kanuga N, Romero IA, Greenwood J, Luthert PJ, Cheetham ME. Oxidative stress affects the junctional integrity of retinal pigment epithelial cells. *Invest Ophthalmol Vis Sci*. 2004;45:675–684.
141. Chrenek MA, Dalal N, Gardner C, et al. Analysis of the RPE sheet in the rd10 retinal degeneration model. *Adv Exp Med Biol*. 2012;723:641–647.
142. Daniele LL, Sauer B, Gallagher SM, Pugh EN, Jr, Philp NJ. Altered visual function in monocarboxylate transporter 3 (Slc16a8) knockout mice. *Am J Physiol Cell Physiol*. 2008;295:C451–C457.
143. Yu C, Lad EM, Mathew R, et al. Microglia at sites of atrophy restrict the progression of retinal degeneration via galectin-3 and Trem2 interactions. *bioRxiv*. 2023, https://doi.org/10.1101/2023.07.19.549403.
144. Kim Y, Tarallo V, Kerur N, et al. DICER1/*Alu* RNA dysmetabolism induces Caspase-8–mediated cell death in age-related macular degeneration. *Proc Natl Acad Sci USA*. 2014;111:16082–16087.

Investigative Ophthalmology & Visual Science